

Master's thesis

2022

Jedrzej Czesak

Master's thesis

**NTNU**  
Norwegian University of  
Science and Technology  
Faculty of Engineering  
Department of Structural Engineering

Jedrzej Czesak

# Behavior of Post-Tensioned concrete box girder with multiple damaged tendons

A Case Study of the Sykkylvsbrua

January 2022





Norwegian University of  
Science and Technology

# Behavior of Post-Tensioned concrete box girder with multiple damaged tendons

A Case Study of the Sykkylvsbrua

**Jedrzej Czesak**

Department of Structural Engineering

Submission date: January 2022

Supervisor: Daniel Cantero

Norwegian University of Science and Technology  
Department of Structural Engineering







NORWEGIAN UNIVERSITY OF SCIENCE AND  
TECHNOLOGY

FACULTY OF ENGINEERING DEPARTMENT OF  
STRUCTURAL ENGINEERING

---

Master's thesis in Civil and Environmental Engineering

Supervisor: Daniel Canterom

---

*Author:*


Jedrzej Jozef Czesak

January, 2022



## MASTER THESIS 2022

SUBJECT AREA: Non-linear analysis of prestressed concrete	DATE: 31.01.2022	NO. OF PAGES: 84
--------------------------------------------------------------	------------------	------------------

TITLE: Behavior of Post-Tensioned concrete box girder with multiple damaged tendons A Case Study of the Sykkylvsbrua in Møre og Romsdal county.	
BY:  Jedrzej Jozef Czesak	

SUMMARY:  The main purpose of this master thesis was to investigate the damages in simply supported box girder bridges. The was carried out by performing non-linear analysis in the Finite element analysis program DIANA FEA 10.5  The thesis is divided into two main parts. First part was based on the recreation of experiments to gain greater knowledge of the program. The modelled experiments were four-point bending tests performed on 2D ordinary reinforced beam and 3D ordinary reinforced slab with post-tensioned. For the second part of this thesis, half span of Sykkylvsbrua was modelled and loaded with self weight and traffic load in addition to the post tensioning load to inspect how damages in embedded active reinforcements affects concrete structures. A numerical model has been created to simulate damages in post-tensioned concrete beams and box girder.  Trondheim 2022
--------------------------------------------------------------------------------------------------------------------------------------------------------------------------------------------------------------------------------------------------------------------------------------------------------------------------------------------------------------------------------------------------------------------------------------------------------------------------------------------------------------------------------------------------------------------------------------------------------------------------------------------------------------------------------------------------------------------------------------------------------------------------------------------------------------------------------------------------------------------------------------------------------------------------------------

RESPONSIBLE TEACHER: Associate professor Daniel Cantero SUPERVISOR(S): Associate professor Daniel Cantero CARRIED OUT AT: Department of Structural Engineering
----------------------------------------------------------------------------------------------------------------------------------------------------------------------

---

## Abstract

The main purpose of this master thesis was to investigate the damages in simply supported box girder bridges. The was carried out by performing non-linear analysis in the Finite element analysis program DIANA FEA 10.5

The thesis is devided into two main parts. First part was based on the recreation of experiments to gain greater knowledge of the program. The modelled experiments were four-point bending tests performed on 2D ordinary reinforced beam and 3D ordinary reinforced slab with post-tensioned. For the second part of this thesis, half span of Sykkylvsbrua was modelled and loaded with self weight and traffic load in addition to the post tensioning load to inspect how damages in embedded active reinforcements affects concrete structures. A numerical model has been created to simulate damages in post-tensioned concrete beams and box girder.

Trondheim 2022

---

# 1 Sammendrag

Hovedformålet med denne masteroppgaven var å undersøke skadene i enkelt støttede boksbjelkerbroer. Dette ble utført ved å utføre ikke-lineær analyse i Finite element-analyseprogrammet DIANA FEA 10.5

Oppgaven er delt inn i to hoveddeler. Første del var baserer seg på å gjenskape forsøk funnet i forskningsartikler for å få nærmere kjennskap til programmet. Forsøkene som ble modellert var firepunkts bøyetester på en todimensjonal etteroppspente bjelke , og to tredimensjonale etteroppspente bjelker. For andre del av denne oppgaven ble halv-spenn av Sykkylvsbrua modellert og belastet med egenvekt og trafikklast i tillegg til etterspenningslasten for å inspisere hvordan skader i innstøpte aktive armeringer påvirker betongkonstruksjoner.

Trondheim 2022

---

# Innhold

<b>1</b>	<b>Sammendrag</b>	<b>3</b>
<b>2</b>	<b>Preface</b>	<b>1</b>
<b>3</b>	<b>List of symbols</b>	<b>2</b>
<b>4</b>	<b>Introduction</b>	<b>4</b>
<b>5</b>	<b>Theory</b>	<b>5</b>
5.1	Prestressed Concrete Bridges . . . . .	6
<b>6</b>	<b>Nonlinear Structural Analysis in DIANA</b>	<b>8</b>
6.1	Applications of FE analysis . . . . .	8
6.1.1	Advantages of nonlinear analysis: . . . . .	8
6.1.2	Disadvantages of nonlinear analysis: . . . . .	8
6.2	Materials constitutive laws . . . . .	8
6.2.1	Concrete . . . . .	9
6.2.2	Reinforcements . . . . .	9
6.2.3	Other material models . . . . .	10
6.3	Finite element types and meshing . . . . .	11
6.3.1	Arc length control . . . . .	12
6.4	Bond-slip vs embedded reinforcements . . . . .	12
6.5	Embedded bar reinforcement concept . . . . .	12
6.6	Introduction to the following chapters . . . . .	13
<b>7</b>	<b>Parametric study of post-tensioned 2D beam with missing tendons</b>	<b>14</b>
7.1	Design of 2D PT beam Specimens . . . . .	14
7.2	Material models . . . . .	16

---

7.3	Numerical iterative procedures . . . . .	18
7.3.1	Structural Nonlinear Analysis . . . . .	18
7.4	Results . . . . .	19
7.4.1	Displacement . . . . .	19
7.4.2	Crack widths . . . . .	20
<b>8</b>	<b>Parametric study of post-tensioned 3D specimen with missing tendons</b>	<b>22</b>
8.0.1	Design of 3D PT beam specimen . . . . .	22
8.0.2	Material models . . . . .	25
8.0.3	Numerical iterative procedures . . . . .	26
8.0.4	Modeling of 3D beam . . . . .	27
8.0.5	Failures in tendons . . . . .	30
8.1	Parametric study of post-tensioned slab with missing tendons . . . . .	32
8.1.1	Design of PT Slab specimen . . . . .	32
8.1.2	Material models . . . . .	35
8.1.3	Numerical iterative procedures . . . . .	35
8.1.4	Modeling of 3D slab . . . . .	36
8.1.5	Results . . . . .	37
<b>9</b>	<b>Sykkylvsbrua</b>	<b>39</b>
9.1	General information . . . . .	39
9.2	Modelling of the post-tensioned beam bridge . . . . .	40
9.2.1	Bridge cross section . . . . .	40
9.2.2	Bridge reinforcements . . . . .	41
9.3	Boundary conditions and constraints . . . . .	42
9.4	Material properties of the bridge model . . . . .	43
9.4.1	Loads . . . . .	43

---

---

9.4.2	Self weight . . . . .	43
9.4.3	Traffic loads . . . . .	43
9.4.4	Prestressing force . . . . .	46
9.4.5	Material properties of the bridge model . . . . .	47
9.5	Material models . . . . .	48
9.5.1	Numerical iterative procedures . . . . .	49
9.6	Meshing and analysis of the bridge model . . . . .	49
<b>10</b>	<b>Results from bridge model analysis</b>	<b>50</b>
10.1	Deflection . . . . .	50
10.1.1	Concrete Cracks Patterns . . . . .	55
<b>11</b>	<b>Summary</b>	<b>56</b>
11.1	Commentary . . . . .	56
11.2	Conclusion . . . . .	56
11.3	Future work . . . . .	57
	<b>Referanser</b>	<b>58</b>
	<b>Appendix</b>	<b>60</b>
<b>A</b>	<b>Appendix</b>	<b>60</b>
A	Midspan deflection in three point bending test . . . . .	60
B	Midspan deflection in four point bending test . . . . .	60
C	Analytical calculations of the RC beam . . . . .	61
C.1	Deformations and cracking load of Stage I of the RC Beam . . . . .	61
D	Reinforcement . . . . .	62
E	Numerical studies of Sykkylsbrua . . . . .	65
E.1	Cross-Sectional Area . . . . .	65

---

---

E.2	1. Areal of moment . . . . .	65
E.3	Area center . . . . .	66
E.4	Second moment of area . . . . .	66
E.5	Loads . . . . .	67
E.6	Statically Indeterminate Beam . . . . .	68
E.7	Displacement . . . . .	69
E.8	Moment . . . . .	69
E.9	Prestressing force . . . . .	69
F	Drawings . . . . .	71



---

## 2 Preface

This master thesis is written as the final part of a five year long master's degree programme at the Norwegian University of Science and Technology (NTNU) at the Department of Structural Engineering. Daniel Cantero was the supervisor of this thesis

Through this assignment, I have gained better understanding of bridge design as well the finite element analysis. I have also gained good knowledge of how failures in tendons can affect bridges. The work has been challenging but rewarding. It has gone a lot of time to learn and use the FEM software Diana FEA, but after a lot of trying I have gained a good understanding of how the program should be used. I am looking forward to use this knowledge in professional life.

I would like to thank my supervisor Daniel Cantero for technical assistance, regular meetings and guiding me through the thesis work.

---

### 3 List of symbols

#### Latin upper case letters

$A_c$	Crosssectional area of concrete
$A_p$	Crosssectional area of prestressing steel
$A_s$	Crosssectional area of passive reinforcement
$E$	Young's modulus
$E_c$	Modulus of elasticity of concrete
$E_p$	Modulus of elasticity of prestressing steel
$E_s$	Modulus of elasticity of reinforcing steel
$G_c$	Concrete compressive fracture energy
$G_F$	Concrete tensile fracture energy
$P$	Prestressing force after immediate losses
$P_{max}$	Jacking force
$R$	Reaction force

#### Latin lower case letters

$e$	Eccentricity
$f_{cc}$	Compressive strength of concrete
$f_{cd}$	Design value of concrete compressive strength
$f_{ck}$	Characteristic compressive cylinder strength of concrete at 28 days
$f_{cm}$	Mean value of concrete cylinder compressive strength
$f_{ct}$	Tensile strength of concrete
$f_{p0,1}$	0,1% proofstress of prestressing steel
$f_p$	Tensile strength of prestressing steel
$f_{fy}$	Yield strength of reinforcement
$f_{fyd}$	Jacking forceDesign yield strength of reinforcement
$n_1$	Number of notional lanes
$w$	Width of carriageway

---

### Greek lower case letters

$\alpha_{cc}$	Coefficient used to calculate the concrete compressive strength
$\gamma_c$	Partial factor for concrete
$\gamma_s$	Partial factor for steel
$\Delta\epsilon_p$	Change of strain for the prestressed reinforcement
$\epsilon_{p0t}$	Initial tensile strain of the prestressed reinforcement
$\epsilon_{p'0t}$	0,1% proofstress of prestressing steel
$\epsilon_u$	Resulting tensile strain of the prestressed reinforcement
$\theta$	Angle
$\mu$	Coefficient of friction between the tendons and their ducts
$\nu$	Poisson's ratio
$\rho$	Density
$\sigma$	Stress

---

## 4 Introduction

### Background

Pre-stressed concrete structures produce high strength and resistance compared to the traditional concrete structures. In addition, multiple other advantages are provided by the usage of pre-stressed concrete such as the faster construction rates, saving of material and preservation of the sustainability concept in the construction area. The objective of this thesis is to study failure in post-tensioned box girder.

### Research methodology

Before modeling the bridge and conducting the nonlinear analyses, to ensure a successful results a literature study of the different function in DIANA was performed. The main source of knowledge was tutorials placed on the official website of the software developer as well documents provided by supervisor. To further ensure that modelling was done correctly, it was decided to first recreate experimental results from provided research articles before a more advanced generic bridge model could be made. Analytical calculations were made to control the numerical calculations.

### About DIANA FEA

DIANA FEA is a multi-purpose finite element program with wide field of application. Developed by engineers from a civil engineering perspective, Diana's most appealing capabilities are in the fields of concrete and soil. DIANA FEA is extensively used for designing and analysis of bridges, road, tunneling and others engineering structures, both linear and nonlinear analysis can be performed in DIANA as well other design checks. (DIANA strongest points lie in its nonlinear capabilities) [1]

### Thesis content

The work consists of 13 chapters that are intended to best present the development of the work. The first chapters presents basic theory related to prestressing concrete. The next chapters is about modelling as well carrying out non linear analysis in DIANA FEA software. Chapters 7 to 8 presents a numerical simulation of a 2D and 3D post tensioned concrete specimens under increasing static load until its failure. Main purpose of those chapters was to study how damages in tendons can lower carrying capacity of the beam. The last chapters of this thesis focus on the main purpose of this master thesis namely to investigate the damages in Sykkylsbrua.

---

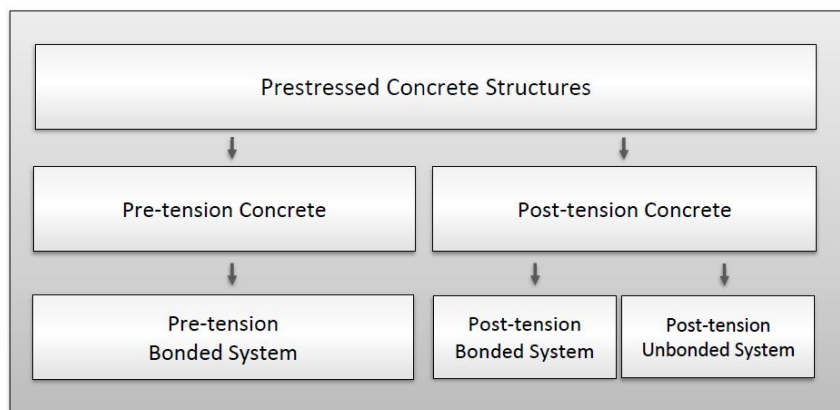
## 5 Theory

This chapter contains the background information about post-tensioned concrete :

Concrete is mainly strong in resisting the compressive stresses while it is weak in resisting tensile stresses. Concrete's tensile strength is almost 10% of the concrete compressive strength this means that any concrete construction that may be subjected to tensile stress must be reinforced with high tensile strength materials such as steel. Concrete needs reinforcement to add tensile strength and to change the failure mode from brittle to ductile. Steel is used as reinforcement because of its strength, its similar thermal behavior, its availability and low cost. The weakness of the steel is that it rusts, it leads to reduction of load capacity of concrete specimens. Additionally rust produces iron oxide that has a higher volume than steel and induces concrete cracking. In fact, corrosion of embedded steel reinforcement is the most common form of concrete deterioration.

Prestressing concrete is a relatively new technology that provides concrete members with higher flexural and tensile strength than traditional concrete. Prestressing concrete is normally accomplished by tensioning the reinforcement within the concrete. This gives the member a compressive stress that will balance the tensile stresses imposed in the member once it is put into service. Prestressing concrete takes advantage of the structural strength of the member in higher grade than conventional reinforcement and thus the prestressing technology employs a less amount of materials usage and a significant reduction in the structure's embodied energy [2]. When the reinforcement is prestressed within concrete this doesn't necessarily lead to an increase in its strength but significantly reduces its deflection. Adding force to the beam is not creating tension, but just reducing the compression that's already been introduced through the tension in the steel rods.

Prestressed concrete members can be either pre-tension or post-tension. A post-tensioned (PT) concrete member can be reinforced with either bonded or unbonded prestressing tendons. Figure below shows the different types of PT concrete members.



Figur 1: Prestressed concrete system

---

In pre-tension concrete tension is put on the steel reinforcement tendons as the concrete is cast. Once the concrete cures, the tension will remain inside, transferring a compressive stress to the concrete through friction with the reinforcement. Pre-tension concrete system can only be bonded system because the concrete is poured around the tendons after the tendons stressing and the stresses are transferred through the created bond to the concrete. Pre-tension system are more suitable for prefabricated element therefore they are usually made at precast plants.

Another way to prestress reinforcement is called post-tensioning in this method, the stress in the reinforcement is developed after the concrete has cured. Concrete elements are cast with empty ducts with their design profile after the concrete reach its desired concrete compressive strength, steel strands are inserted. Next, the tendons are stressed with the aid of hydraulic jacks and are anchored to the concrete's surface using mechanical anchorage devices and then the tendons are cut. For cast in suite elements such as slab and beam the post-tensioning technique provides premium advantages when compared to the pre-tension system. The post-tension system ensures the integrity between the different elements of the structure through the continuity of the tendon and the structure's continuous framing additionally post-tension systems eliminate joint troubles as this system provides a monolithic connection between the different members of the structure. [3]

There are two types of post tensioning one is bonded and the other is unbonded system. In unbonded system ducts contain oil or grease and the anchors are covered with grout where in bonded post-tension structures are made of plastic or steel ducts in which the steel tendons are placed. Unbonded has this advantages over bonded system that its allows retightening strands. In bonded system the ducts are filled with grout after stressing to create a bond between strand and the duct. After grout is cured the relative movement between the tendon and the concrete is no longer possible.

## 5.1 Prestressed Concrete Bridges

There are many types of modern concrete bridges, generally they can be broken down into three main categories: plain or unreinforced concrete, reinforced concrete and prestressed concrete. Due to the various advantages that the prestressing technology offers its different variants are used in various situations.

Pre-tensioning method is commonly used for precast beam bridges. Usually tendons in pre-tensioning beam are straight and bridges are most single span bridges with span length ranging to about 20 meters at a maximum

Post-tensioning is commonly used for voided decks and box girders to long span (more than 30 meters). The post-tension system is used also in many rehabilitation application

---

of old or deteriorated buildings.

Need for post-tensioned box girder bridges:

- High torsional resistance of box sections which beneficial for the beneficial for horizontally curved bridges
- Material cost cutting. Post-tensioning leads to reduction in concrete member size and rebars this is because the steel is in tension and that is basically pushing the concrete into compression
- Lower overall maintenance and life cycle costs of the structure. Only when we take carry out grouting properly manner.(monitoring of the actual site when it is being carried out)
- Higher ultimate strength due to bond generated between the stand and concrete in both compression and tension. Grouting of the cables and the interaction between the steel in tension and concrete in compression
- Full section utilisation (crack controll)

Types of box girder bridges: There are 4 major methods of construction

- Segmental Construction
  - Balanced Cantilever Method Box girder segments are added to either side of the pier table to balance each other out. During the construction the segments together behave as a cantilever supported at the pier table location.
  - Incremental Launching Method Construction is done with the help of a launching steel girder also know as the nose. The segments are cast in-situ and as segments are cast behind the launching girder they are pushed by sliding mechanism from one abutment to the other. (Useful only for straight bridges)
- Span by Span Method of Construction
  - Full Staging Method Dead weight of concrete, formwork and falsework are fully shored or staged over the full spans of the bridge until concrete gains a certain level of strength. Each segment is constructed sequentially span by span. Use of continuous tendon is limited for long spans. Structural Analysis is done on the basis of construction stages defined by construction joints.
  - Movable Scaffolding Method The scaffold moves as it builds one span at a time

---

## 6 Nonlinear Structural Analysis in DIANA

### 6.1 Applications of FE analysis

#### 6.1.1 Advantages of nonlinear analysis:

Advanced software empower engineers to provide adjusted predictions to non-linear concrete behaviour as cracking and deflection.

Nowadays, thanks to the capability of solvers and computers it is possible to define, analyze and simulate the non-linear behaviour of complete structures with a reasonable calculation time [4]

#### 6.1.2 Disadvantages of nonlinear analysis:

Non-linear FE analysis require a deep understanding and awareness of its limitations is needed so that it can be properly applied. Incorrect model definition or not properly chosen solution procedures can lead to convergence issues and then to an incorrect answer. [5].

Performing nonlinear analysis is far more challenging then linear analysis because each non linear problem is unique in its rights and there is not one unique solution procedure that is suitable for all problems. Because of it principles such as principle of superposition can no longer be applied and only one load situation can be handled at a time.

### 6.2 Materials constitutive laws

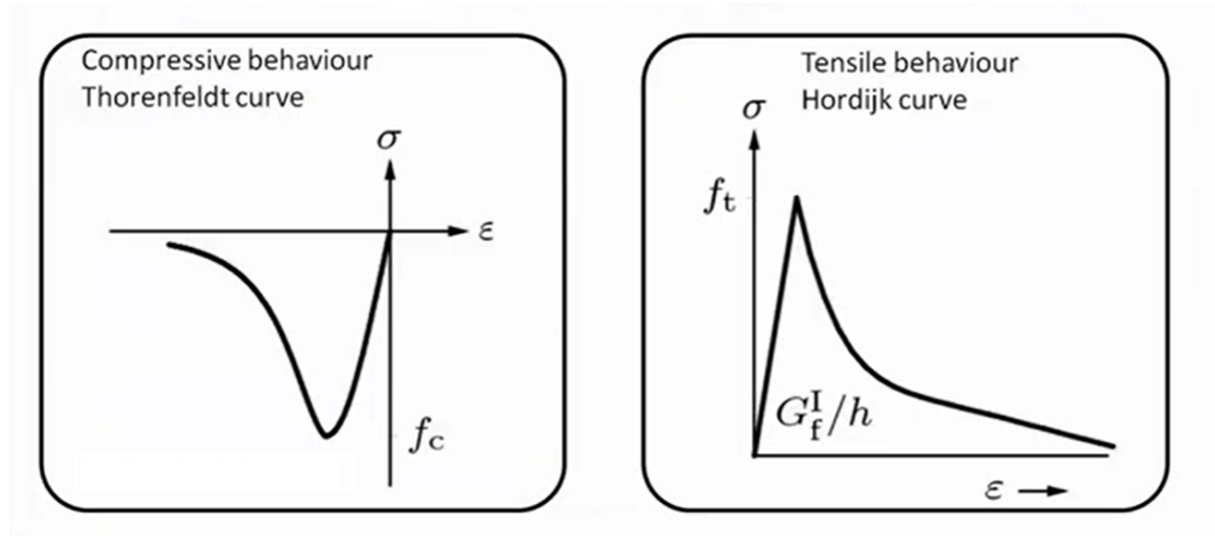
One of the things that it is important while analyzing a structure with help of FE analysis is to define a material constitutive laws knows also as material modes. They are simplified abstractions of the true material behaviour and are used in a finite element context to specify the stress strain relationship, that is assumed forthe materials in the structure.[6]



---

### 6.2.1 Concrete

For the concrete a total strain crack model were used



Figur 2: Thorenfeldt and Hordijk curve

Compressive behavior of the concrete is based on Thorenfeldt curve and the strength compressive resistance of the concrete is the long term resistance. For the tensile behaviour, Hordijk curve was selected.

The fracture energy of concrete  $G_F[N/mm^2]$ , defined as the energy required to propagate a tensile crack of units area, should be determined by test. Model is based on information provided in the construction project. In the absence of experimental data  $G_F[N/mm^2]$  was estimated as:

$$G_f = 73 \cdot f_{cm}^{0.18} \quad \text{where} \quad f_{cm}^{0.18} = \text{is the mean compressive strength in MPa}$$

### 6.2.2 Reinforcements

For the reinforcement an elastoplastic material curve was used. In DIANA, this nonlinear model is called the Von Mises plasticity model. Figure below shows the idealized stress-strain diagram for a Pre-stressed reinforcement which is recommended in Eurocode 2.

This diagram is applied both for tensile and compressive stresses. The material response is linear up until the yield point  $f_{p,01}$ , with an elastic modulus  $E_p$ . When the yield stress is surpassed according to the Von Mises yield criterion, the ductile phase begins. In DIANA when defining the ductile behaviour for reinforcement user can chose a hardening function. For the "no hardening" option, no point of failure is specified and the yield stress is the

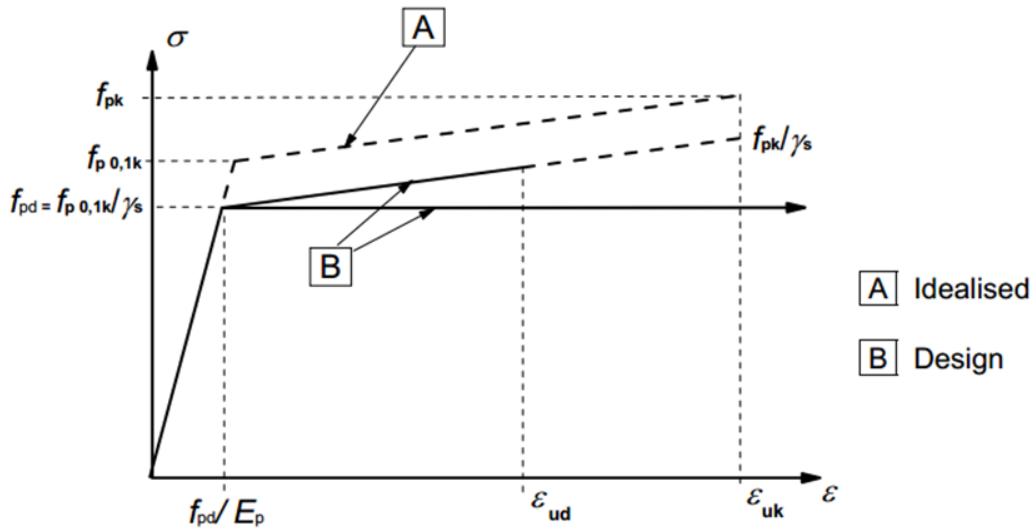


Figure 3: Idealised and design stress-strain diagrams for prestressing steel

maximum appearing stress giving a horizontal top branch without strain limit. in the diagram. The ductile behaviour can also be modelled as an inclined branch, with a defined point of failure at the strain limit  $\epsilon_u$  with a maximum stress  $f_p$ . [7]

### 6.2.3 Other material models

In accordance with the advice from tutorials provided by DIANA software producer a set of support and load plates were modelled together with concrete structures. This was done to avoid instant cracking at the point where load was applied.

To ensure a successful results and attach different type material to each other an interface was defined between concrete beam and steel support. An interface material was defined by using a nonlinear elasticity model. Support was modelled as a roller support with low values for the shear stiffness modulus in x and y directions and a high value for the compressive normal stiffness in z direction. Such definition of values allows concrete to move relative to the steel plate in the horizontal direction. The model "Notension with shear stiffness reduction" is used, to ensure that the steel plate does not transfer any tensile forces to the concrete surface. Interface opening was selected to be 0.001 mm

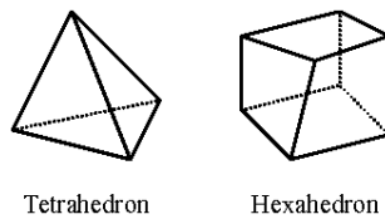
---

## 6.3 Finite element types and meshing

In finite element modeling, a model is divided and discretized into a system of elements. For each element is solved by numerical equations, which together give the global reaction on the model. To capture the right behavior of the discrete model, it is therefore important to use suitable items with correct number of nodes and degrees of freedom. The choice of element types depends on whether the project is modelled in two or three dimensions. The relevant finite elements for this thesis are the plane stress elements, which are used in two dimensional modelling, and the three dimensional solid elements.

Plane stress elements is defined only in the xy plane. This type of element can be used for three dimensional models by defining constant thickness  $t$  in the z direction providing that the out of plane stress components in all directions are zero. This means that the model can only be loaded in the plane of the element. The advantage with plane stress elements is that it allows a faster finite element analysis, as the stiffness matrices are reduced to a size of  $3 \times 3$ . [7]

There are two main types elements for continuum solid elements in 3D, one is tetrahedral and the other is hexahedral elements, shown under. The tetrahedrons are versatile pyramid-like elements where hexahedrals are cubic elements. The stiffness matrices include translation and rotation about all three axes, which is particularly important when the loading directions are arbitrary. With cube-shaped hexahedres, one generally experiences an equally accurate solution as with tetrahedrons, but to a lower cost due to better convergence.



Figur 4: The two types of mesher type elements in DIANA

**The Q8MEM element**, which is a four nodal isoparametric plane stress element, has been used for the 2D modelling in this thesis.

**The HX24L element**, which is a type of solid element, has been used for the 3D modelling in this thesis.

---

### 6.3.1 Arc length control

Arc length control is used to follow the path of response with automatic scale of load steps. In the regular arc length control settings consider the translations in the Y direction because it is the direction of loading for 2D beam or Z direction for 3D beam. To control the arc length the nodes of the loading steel plate was chosen, are representative of the dominant displacement response.

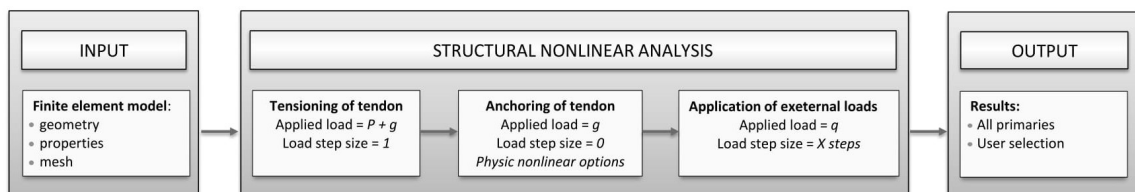
## 6.4 Bond-slip vs embedded reinforcements

DIANA offers two methods for the modeling of pre- or post-tensioning behavior of tendons in concrete: Direct method and indirect method

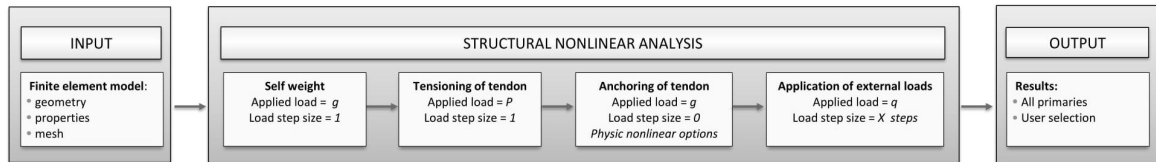
- Case 1 – Post tensioning with embedded rebars: For practical analyses of post-tensioned RC structures in which the loss of prestress due to friction and penetration of the anchorage in the concrete are predicted indirectly using an analytical model.
- Case 2 – Post tensioning with bond slip rebars: For detailed analyses of post-tensioned RC structures in which the loss of prestress due to friction is modeled directly with a bond slip model and the anchor plate is also modeled. Model definition

## 6.5 Embedded bar reinforcement concept

Mesh: Tendon is modeled as line and assigned with embedded bar reinforcement property.  
Load: Post-tensioning load is applied directly with a special load type for post-tensioned reinforcement. Post-tensioning load can be applied together with self weight or separately, the chosen method does not affect the results.



Figur 5: Embedded reinforcement concept 1



Figur 6: Embedded reinforcement concept 2

## 6.6 Introduction to the following chapters

Next three chapters of this thesis describes how bending tests on post tensioned beams with different geometry were modelled in DIANA. All models were based on published experimental results with the same geometry and loading procedure. Models were tested multiple times and checks to ensure validity and representative of results.

- Chapter 7 focus on the methodology for the modelling and analysis of the 2D reinforced concrete beam. Which than was modified and passive reinforcement located in the lower part of beam was replaced with active reinforcement. The main purpose of chapter was to gain a greater knowledge of the program by modeling simple 2D case.
- Chapter 7 Part I presents a numerical simulation of a 3D post tensioned concrete beam under increasing static load until its failure. To ensure that the modeling and analysis were representative, two beam with fully prestressing case (31.1 KKN) and two with the partial prestressing force (15.1KKN) were compared with previous literature study. After verifying that the model generated in DIANA is acceptable a new set of beam was modelled and a new series of test have been carried out in which the tendons were gradually damaged. Than main purpose of chapter was to study how damages in tendons can lower carrying capacity of the beam.
- Chapter 8 Part II describes the general modelling method used for the 3D post tensioned concrete slab. The main purpose was to study damages in simply supported slab and to evaluate what is the effect of having a damaged post-tension system. The second goal was to consolidate knowledge of the program before modeling Sykkylvsbrua in DIANA.
- Chapters from 9 - 13 focus on the methodology for the modelling and analysis of Sykkylvsbrua. The goal was to evaluate what is the effect of having a damaged post-tension system in a typical box girder bridge.

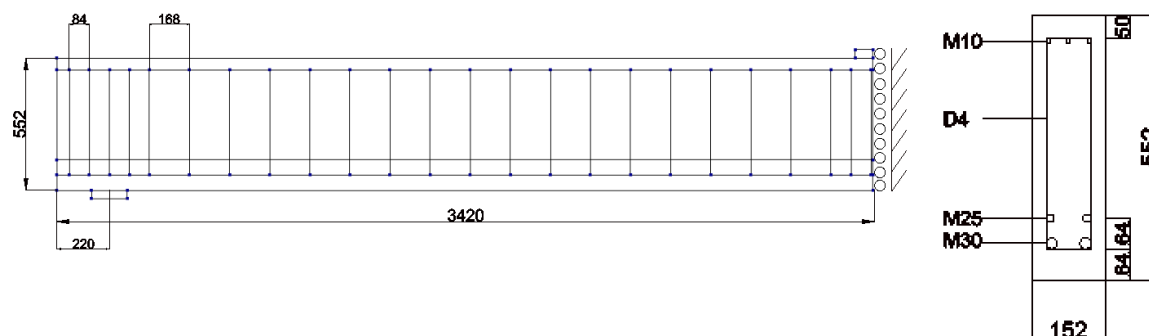
---

## 7 Parametric study of post-tensioned 2D beam with missing tendons

### 7.1 Design of 2D PT beam Specimens

This part presents a numerical simulation of a post-tensioned 2D beam under increasing static load. The starting point was DIANA tutorial [*Reinforced Concrete Beam: Simulation of an Experimental Test*][8] that presents a numerical simulation of an experimental test on a reinforced concrete specimen VS-C4 from the series of experiments carried out in the University of Toronto by Vechino and Shim (2004). The beam was modified and passive reinforcement M25 located in the lower part of beam was replaced with active reinforcement, the dimension of reinforcement M25 remained the same.

The beam has a total length of 6.840 m, a depth of 0.552 m, and a width of 0.152 m. The geometry, reinforcement, loading, boundary conditions and experimental set-up are presented in figure under.



Figur 7: Geometry and reinforcements of the beam based on specimen VS-C3

The beam exhibited a flexural-compressive failure mode. The measured peak load for RC without post-tensioned was  $P_{exp} = 265$  kN at a deflection of 44.3 mm.

As the beams have a simple rectangular crosssection, they were modelled in two dimensions, using plane stress finite elements. Due to symmetry, only half of the beam is modeled. The concrete response is simulated with a total strain rotating crack model. The reinforcement steel is modeled with hardening plasticity. The steel plates for load application and support are also modeled with linear elastic material properties. Interface elements are used between the steel plates and the concrete beam. A static nonlinear analysis is performed with increasing imposed displacement until failure. Coarser mesh and default integration settings was used

Tabell 1: Material properties

<b>Concrete</b>	
Young's modulus $E$	34300 $N/mm^2$
Poisson's ratio $\nu$	0.2
Compressive strength $f_{cm}$	43.5 $N/mm^2$
Tensile strength $f_{tm}$	3.13 $N/mm^2$
Fracture energy in compression $G_c$	35.975 $N/mm$
Fracture energy in tension $G_F$	0.1439 $N/mm$
Mass density $\rho$	2.4E-9 $T/mm^3$
<b>Reinforcement steel M10</b>	
Diameter $\phi$	11.3 $mm$
Young's modulus $E$	200000 $N/mm^2$
Yielding strength $f_{ym}$	315 $N/mm^2$
Ultimate strength $f_{um}$	460 $N/mm^2$
Ultimate strain $\varepsilon_{su}$	0.025
<b>Reinforcement steel M25</b>	
Diameter $\phi$	25.2 $mm$
Young's modulus $E$	200000 $N/mm^2$
Yielding strength $f_{ym}$	445 $N/mm^2$
Ultimate strength $f_{um}$	680 $N/mm^2$
Ultimate strain $\varepsilon_{su}$	0.05
<b>Reinforcement steel M30</b>	
Diameter $\phi$	29.9 $mm$
Young's modulus $E$	200000 $N/mm^2$
Yielding strength $f_{ym}$	436 $N/mm^2$
Ultimate strength $f_{um}$	700 $N/mm^2$
Ultimate strain $\varepsilon_{su}$	0.05
<b>Reinforcement steel D4</b>	
Diameter $\phi$	5.7 $mm$
Young's modulus $E$	200000 $N/mm^2$
Yielding strength $f_{ym}$	600 $N/mm^2$
Ultimate strength $f_{um}$	651 $N/mm^2$
Ultimate strain $\varepsilon_{su}$	0.05
<b>Steel for plates</b>	
Young's modulus $E$	200000 $N/mm^2$
Poisson's ratio $\nu$	0.3

---

## 7.2 Material models

In the following section are presented properties assignee to material models.

### Concrete

---

When defining the properties for the concrete slab, the Element Class was set to Regular Plane Stress. The concrete material was defined with the properties stated below.

Class:	Concrete and masonry
Material model:	Total strain based crack model
Crack orientation:	Rotating
Tensile curve:	Exponential
Crack bandwidth specification:	Rots
Poisson's ratio reduction model:	No reduction
Compression curve:	Parabolic
Reduction due to lateral cracking:	Reduction model by Vecchio and Collins 1993
Lower bound reduction curve:	0,6
Stress confinement model:	No increase

### Steel plates

---

The steel plate has a total length of 0.150m, a width of 1.000 m and a thickness of 0.350m was selected. Load plates and support plates were defined as.

Class:	Steel
Material model:	Linear elastic isotropic
Elastic modulus:	210000 $N/mm^2$
Poisson's ratio $\nu$ :	0.3
Mass density:	0

### Reinforcement

---

The passive reinforcements of the slab models, including the tendons and stirrups as well active reinforcements, were defined as.

Class:	Reinforcements
Material model:	Von Mises Plasticity
Plastic hardening :	Plastic-strain-yield stress
Hardening hypothesis:	Strain hardening
Haredning type :	Isotropic hardening

Strain-Stress diagram for prestressed reinforcement was defined as Total strain-yield stress. Therefore it differs from the others figures.

---



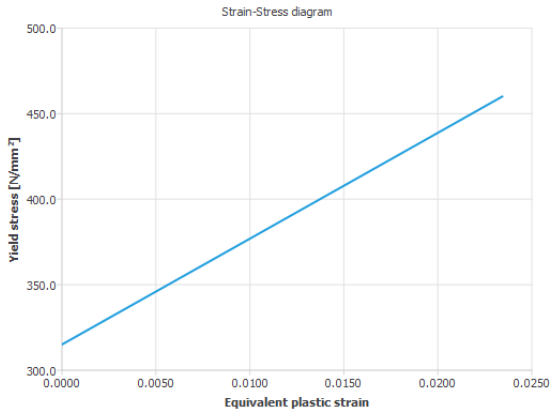


Figure 8: Stress strain curve for M10

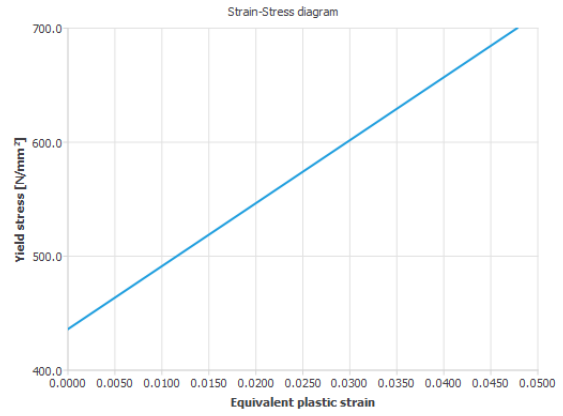


Figure 9: Stress strain curve for M30

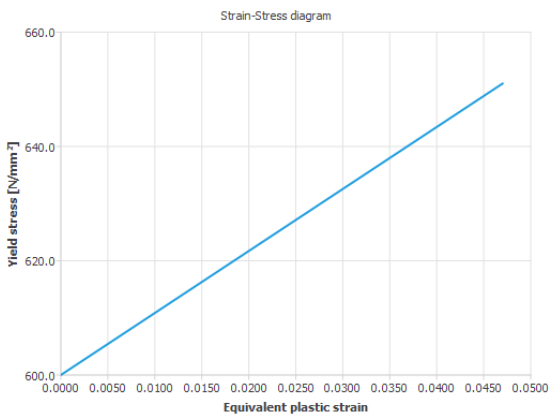


Figure 10: Stress strain curve for stirrups D4

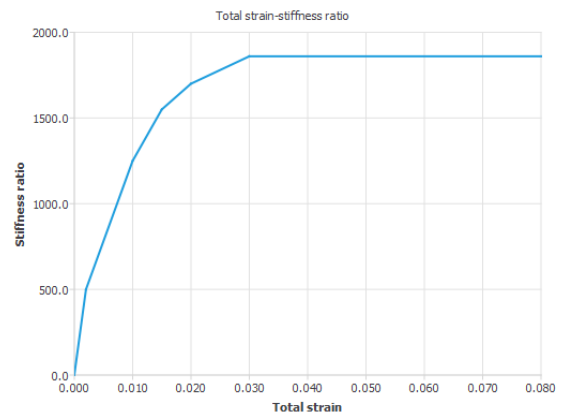


Figure 11: S-S Curve for active reinforcements

## Interface material properties

Surface between slab and steel plates were defined as.

Class:	Interface elements
Material model:	Nonlinear elasticity
Type:	2D line interface
Normal stiffness modulus-y:	34200 $N/mm^3$
Shear stiffness modulus-x:	0,000342 $N/mm^3$
No-tension or diagram:	Notension with shear stiffness reduction
Critical interface opening for reduction:	0,001 mm
SNormal/shear stiffness reduction factor:	0

---

## 7.3 Numerical iterative procedures

The non-linear analyses for the beam models were executed with the Regular Newton-Raphson iteration method. To ensure a reliable results 20 was selected to be maximum number of iteration. Energy convergence criterion was chosen as convergence norm because those norms was used as default setting for RC beam from DIANA tutorial. Convergence tolerance was chosen with 0.005 tolerance and 10000 abort criterion. All others parameters remains on default setting.

### 7.3.1 Structural Nonlinear Analysis

A structural nonlinear analysis until failure by increasing the load has been conducted. Self weight has not been considered in the analysis because of performing an analysis until failure self weight have negligible influence on the performance of the specimen. (However in all later analysis self weight has been considered.) The point load of -1000N in Y direction is applied in 99 steps until failure. Load is multiply with a factor of 5 with each step. Arc length control with regular control type was used. Node between 4332-4344 were selected as DOFs control sets.

---

## 7.4 Results

### 7.4.1 Displacement

The presentation of results with the curve of applied load vs. displacement at mid span.

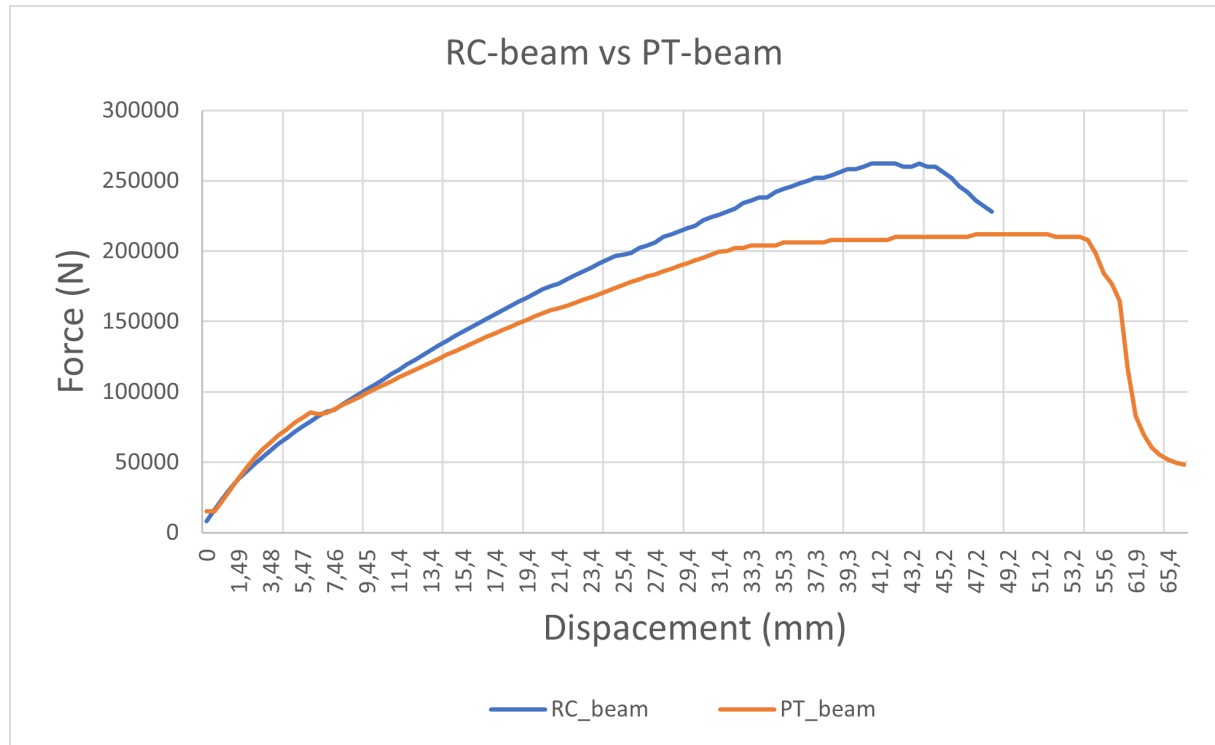


Figure 12: Displacement vs Force diagram

Graph above shows the reaction force versus displacement in Y direction in the bottom part of the beam at mid span for reinforced concrete (RC) beam and post tensioned concrete (PT) beam. Load is the reaction force  $F_{BY}$  multiplied by 2 and deflection is the displacement  $T_{DtY}$  multiplied by -1.

Figure shows when the reinforcement M25 is put under tension the load carrying capacity goes down however maximum displacement for beam is higher. The maximum deflection for the PT beam is around 54.2 mm for RC 44.9mm . The maximum force is 262 kN for RC beam and 212kN for PT beam. The RC beam exhibited a flexural-compressive failure mode where PT beam represent typical flexural-tensile failure mode where the tensile steel yield before the concrete crosses and also it is characterized by large vertical cracks and large deflection. Post-peak response for both beams is captured very well. Both beams at the start behave linearly at point where displacement is 5mm and cracks start to appear both beams start to behave non linearly. Very large plateau for PT-beam indicates a very ductile behavior.

---

### 7.4.2 Crack widths

Largest vertical cracks are appearing as expected at the midspan on the bottom part of the beam, where tensile force are highest. Figures below presents crack patterns view at different beam deflection levels. 5mm, 15mm, 25mm and 45mm points have been selected.

First two figures shows the crack width when total displacement for beam in y direction is 5 mm is the point where the first cracks are registered for both RC and PT beam. The largest crack at this stage is  $2.02 \cdot 10^{-2}mm$  for PT and  $2.18 \cdot 10^{-2}mm$  for RC. At this point the cracks are so small that it would be difficult to register them visually. Cracks for PT beam are slightly larger. Next two figures represent the beam where the cracks are big enough to be detected. The largest crack at this stage is  $0.76mm$  for PT and  $0.65mm$  for RC. Crack patterns start to differ significantly. In the third set of figures crack are opening more the largest crack at this stage for PT beam grew by 55% and doubled for RC from  $0.65mm$  to  $1.33mm$ . Last figures shows RC at the time of failure and PT in its flexural performance mode. Diagonal cracks that run through almost the full height of PT becomes more apparent.

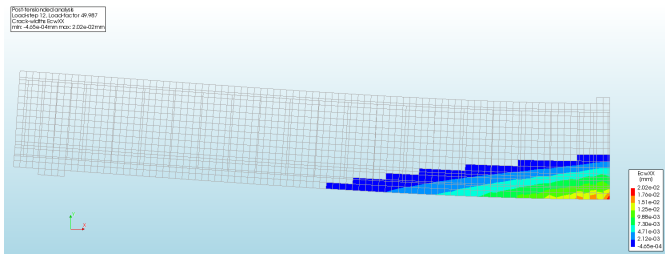


Figure 13: Crack width for PT at 5 mm displacement

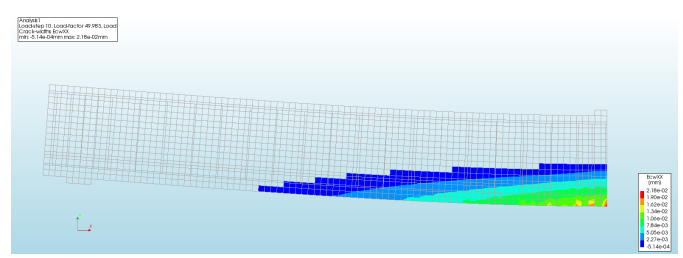


Figure 14: Crack width for RC at 5 mm displacement

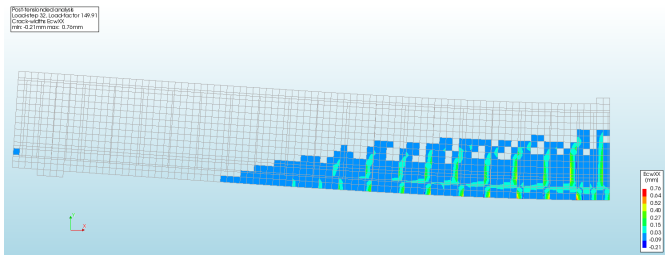


Figure 15: Crack width for PT at 15 mm displacement

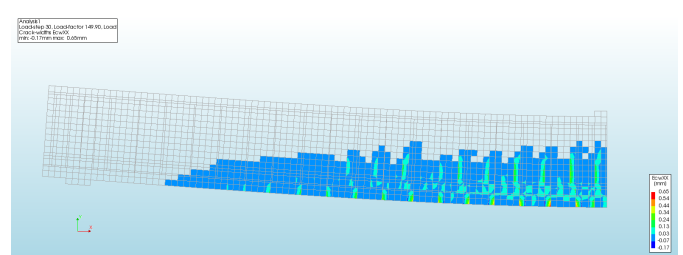


Figure 16: Crack width for RC at 15 mm displacement

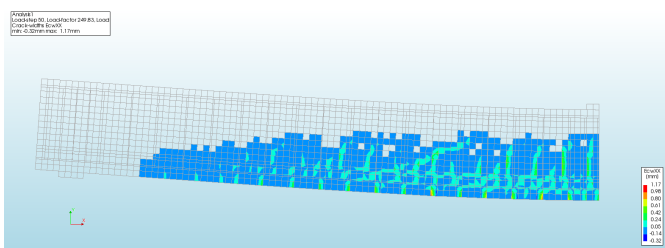


Figure 17: Crack width for RC at 25 mm displacement

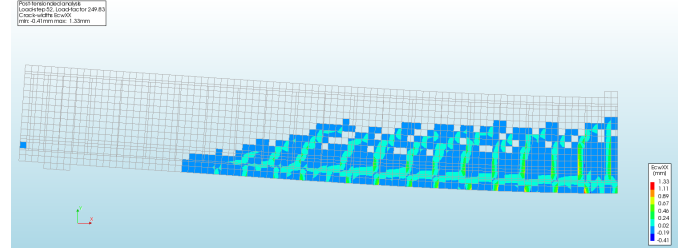


Figure 18: Crack width for PT at 25 mm displacement

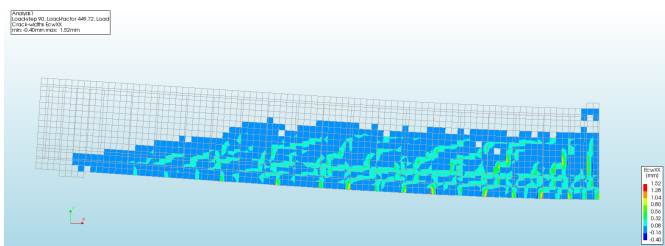


Figure 19: Crack width for RC at 45 mm displacement

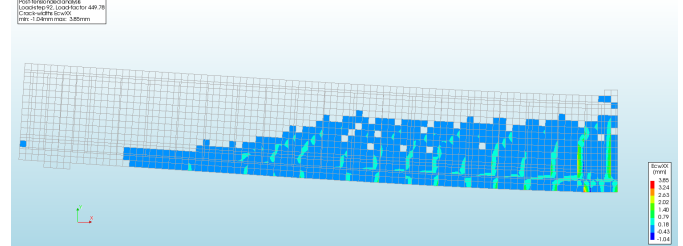


Figure 20: Crack width for PT at 45 mm displacement

---

## 8 Parametric study of post-tensioned 3D specimen with missing tendons

This chapter contains the modeling and analysis of DIANA 3D model. The chapter is divided into two parts. Part I contains details regarding the design, modeling and analysis of 3D beam and part two is dedicated to slab analysis

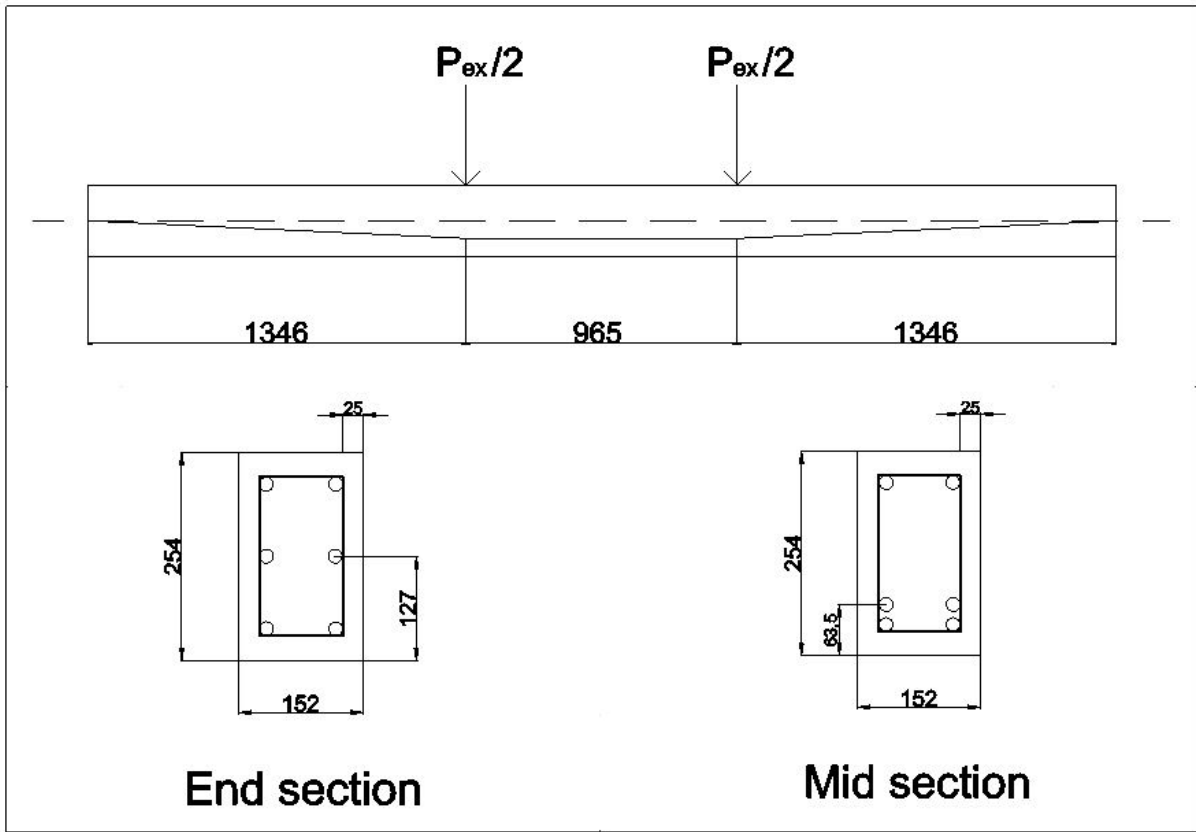
### 8.0.1 Design of 3D PT beam specimen

This part presents numerical simulations of a post-tensioned 3D beam under increasing displacement until failure. The starting point was an article from the International Journal for Research in Applied Science & Engineering Technology [*Nonlinear Flexural behaviour of Post Tensioned Beam*] [9] written by Ajinkya S. Dixit and V.G. Khurd.

The article presents analysis of a post-tensioned concrete beam or determination of physical properties such as deflection, stress distribution under a two-point loading. The researcher used the ANSYS V15.0 Finite Element Analysis tool to analyze the beam. The main objective of the publication was to develop three-dimensional finite element modeling (3D-FEM) of Post-Tensioned Concrete Beam that could be used to investigate the nonlinear response.

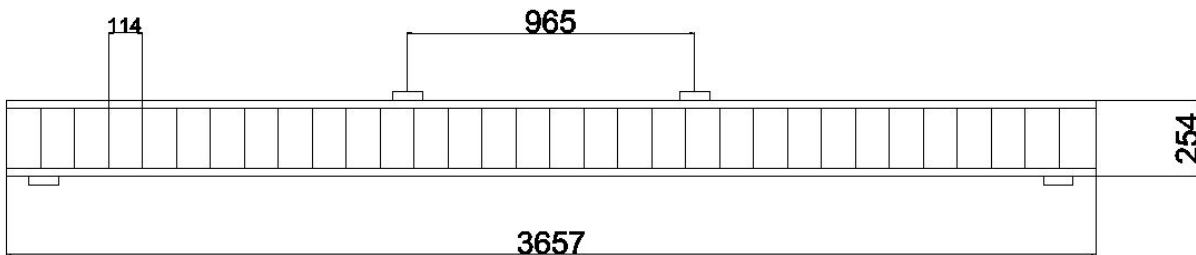
The article was based on studies carried out in 2010 by Kim, U., Chakrabarti, P. R., and Choi, J. H., on unbonded post-tensioned concrete beam. [10]

The beam is simply supported over a span of 3.657 m, a depth of 0.254 m, and a width of 0.152 m. It is subjected to four-point loading. The load is applied through a hydraulic cylinder. The geometry, reinforcement, loading, boundary conditions, and experimental set-up are presented in the figure below.



Figur 21: Typical detail for post-tensioned concrete beam (Kim, U., et al 2010,)

To prevent shear failure 32 vertical stirrups was model. The distance between each stirrup is exactly 114 mm. The most external stirrups has cover depth of 9 mm. The geometry of stirrups are presented in figure under.



Figur 22: Stirrup detail for post-tensioned concrete beam (Kim, U., et al 2010,)

As the beams have a simple rectangular crosssection, they were modelled in three dimensioning. The concrete response is simulated with a total strain rotating crack model. The reinforcement steel is modeled with hardening plasticity. The steel plates for load application and support are also modeled with linear elastic material properties. Interface elements are used between the steel plates and the concrete beam. A static nonlinear analysis is performed with increasing imposed displacement until failure. Hexq/Quad mesh

and default integration settings was used

Tabell 2: Material properties

<b>Concrete</b>	
Young's modulus $E$	32009.30 $N/mm^2$
Poisson's ratio $\nu$	0.2
Compressive strength $f_{cm}$	33 $N/mm^2$
Tensile strength $f_{tm}$	2.56 $N/mm^2$
Fracture energy in compression $G_c$	34.24 $N/mm$
Fracture energy in tension $G_F$	0.14 $N/mm$
Mass density $\rho$	2.4E-9 $T/mm^3$
<b>Reinforcement steel for stirrups</b>	
Diameter $\phi$	5.43 $mm$
Young's modulus $E$	200000 $N/mm^2$
Yielding strength $f_{ym}$	315 $N/mm^2$
Ultimate strength $f_{um}$	460 $N/mm^2$
Ultimate strain $\varepsilon_{su}$	0.025
<b>Reinforcement steel for strands</b>	
Diameter $\phi$	9.53 $mm$
Young's modulus $E$	200000 $N/mm^2$
Yielding strength $f_{ym}$	414 $N/mm^2$
Ultimate strain $\varepsilon_{su}$	0.03
<b>Steel for active reinforcement</b>	
Diameter $\phi$	9.53 $mm$
Young's modulus $E$	200000 $N/mm^2$
Yielding strength $f_{ym}$	1860 $N/mm^2$
Ultimate strain $\varepsilon_{su}$	0.03
<b>Steel plates</b>	
Young's modulus $E$	210000 $N/mm^2$
Poisson's ratio $\nu$	0.3
Mass density $\rho$	8E-9 $T/mm^3$



---

## 8.0.2 Material models

In the following section are presented properties assignee to material models.

### Concrete

---

When defining the properties for the concrete beam, the Element Class was set to Structural Solids. The concrete material was defined with the properties stated below.

Class:	Concrete design codes
Material model:	fib Model Code for Concrete Structures 2010
Aspects to include	Total Strain crack model
Concrete type	Normal weight
Concrete class	C25
Cement type	Normal hardening CE 32.5N
Aggregate type	Quartzite
Air content in %	2

### Reinforcement

---

The passive reinforcements of the beam models, including the stirrups and strands , were defined as.

Class:	Reinforcements
Material model:	Von Mises Plasticity
Plastic hardening:	Total strain-yield stress
Hardening hypothesis:	Strain hardening
Haredning type :	Isotropic hardening

The active reinforcements of the beam were defined in the similarly way, except for the stress-strain curve. Graphs below shows exact stress strain curve for strands and rebars

### Steel plates

---

The steel plate has a total length of 0.100m, a width of 0,1524 m and a thickness of 0.030m was selected. Load plates and support plates were defined as.

Class:	Steel
Material model:	Linear elastic isotropic
Elastic modulus:	210000 $N/mm^2$
Poisson's ratio $\nu$ :	0.3
Mass density:	8E-9 $T/mm^3$

---

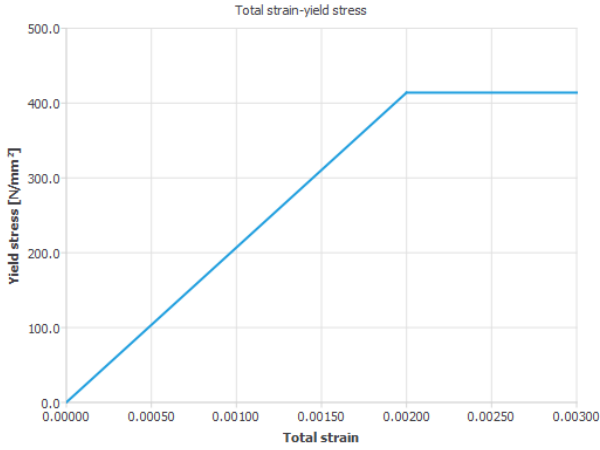


Figure 23: Stress strain curve for stirrups and passive reinforcements

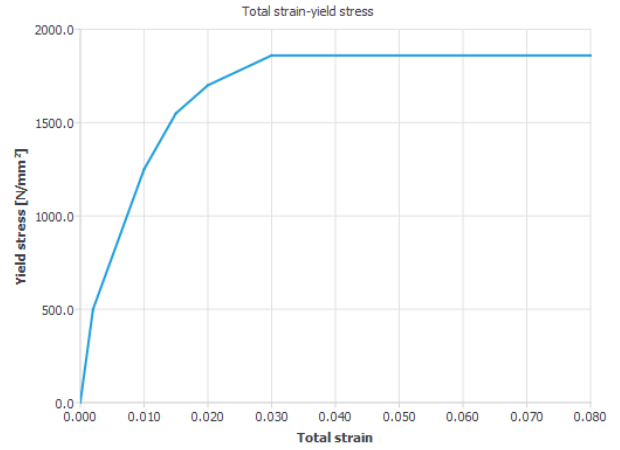


Figure 24: Stress strain curve for active reinforcements

## Interface material properties

Surface between slab and steel plates were defined as.

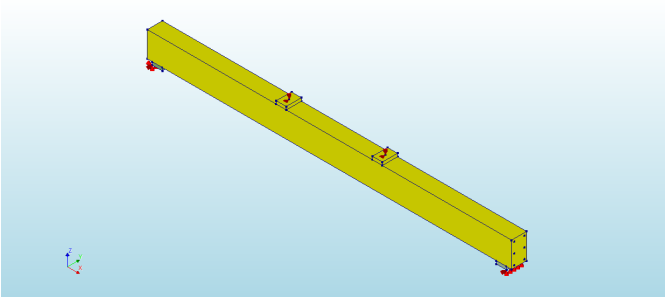
Class:	Interface elements
Material model:	Nonlinear elasticity
Type:	3D surface interface
Normal stiffness modulus-z:	34200 $N/mm^3$
Shear stiffness modulus-x:	0,000342 $N/mm^3$
Shear stiffness modulus-y:	0,000342 $N/mm^3$
No-tension or diagram:	No-tension with shear stiffness reduction
Critical interface opening for reduction:	0,001 $mm$
Normal/shear stiffness reduction factor:	0

### 8.0.3 Numerical iterative procedures

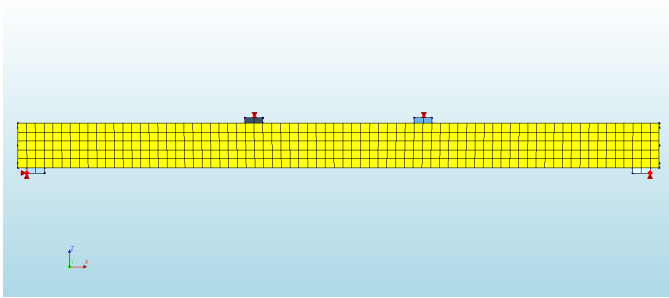
The non-linear analyses for the beam models were executed with the Regular Newton-Raphson iteration method. To ensure a reliable results 20 was selected to be maximum number of iteration. Energy convergence criterion was chosen as convergence norm with 0.005 tolerance and 10000 abort criterion. All others settings remains on default setting.

### 8.0.4 Modeling of 3D beam

Figures below show the geometry of the post tensioned beam with all support and load plates as well as meshing of the model. In order for the nonlinear analysis to be done accurately, the loads are required to have a gradual application. In this experiment, the load was applied until failure, using hydraulic jacks with an incremental application of deflection of -0.1 mm per step. Deflection and the appearance of cracks was measured during experiment.

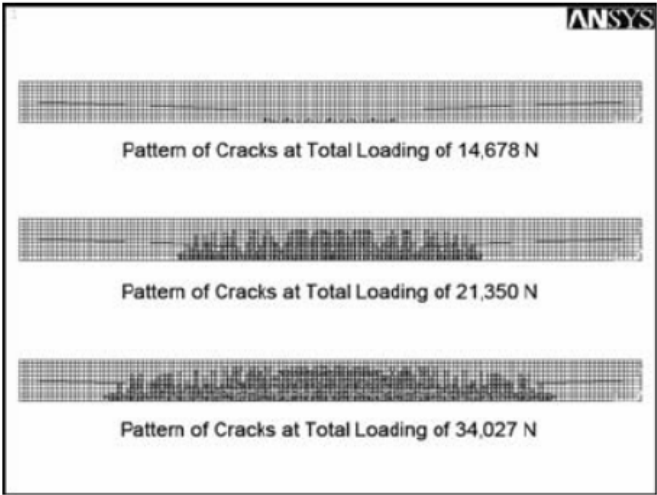


Figur 25: Isometric view of the beam

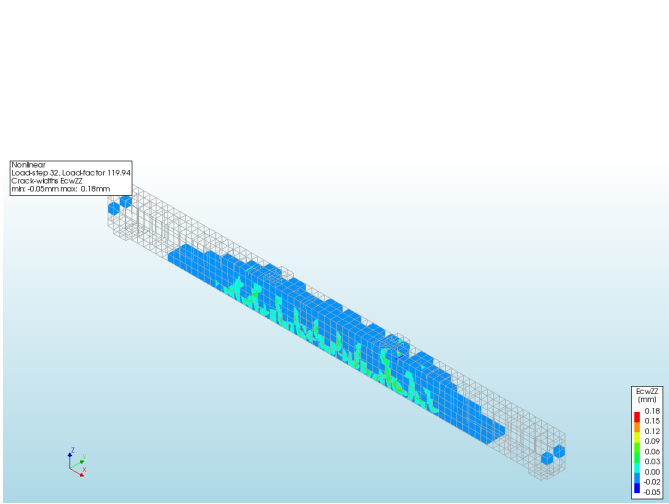


Figur 26: Horizontal view with meshing

An important step in finite element analysis is meshing of the model because mesh size determine the accuracy of the obtained results it is important to select mesh size based on what accuracy is needed. Based on "Guidelines for Nonlinear FEA of concrete structures" a 25.4 cubic mesh size was selected for this model.[11]



Figur 27: ANSYS: Pattern of cracks at total loading of 14,678 N, 21,350 N, and 34,027 N



Figur 28: Crack widths for a beam 2 with applied prestressing force of 31.1kN

Pattern of cracks are similarly for both beams. The maximum crack width of beam at failure in Z plan is 0.28mm and 1.17mm in X plan.

Tabell 3: Beam 1

Deflection (mm)	2,5	12,7	16,2	22,9	27,5
Loas (TEST)	13122	26688	30000	33805	35000
Load (DIANA)	22005	32600	33800	34250	x
Difference	40 %	18 %	11 %	1 %	x
Load (ANSYS)	18014	26243	30000	34250	35000
Load (DIANA)	22005	32600	33800	34250	x
Difference	18 %	20 %	11 %	0 %	x

Tabell 4: Beam 2

Deflection (mm)	2,5	7,5	12,7	15	17,9
Loas (TEST)	10008	16000	22018	24000	27527
Load (DIANA)	16500	20350	25100	26000	26100
Difference	39 %	21 %	12 %	8 %	-5 %
Load (ANSYS)	15568	18300	23130	26000	28956
Load (DIANA)	16500	20350	25100	26000	26100
Difference	6 %	10 %	8 %	0 %	-11 %

Tabell 5: Beam 31.1 kN 3-4

Deflection (mm)	2,5	7,5	12,7	17,5	22,9
Loas (TEST)	12454	21500	30691	38000	44925
Load (DIANA)	21000	31150	40500	48200	48000
Difference	41 %	31 %	24 %	21 %	6 %
Load (ANSYS)	18682	24200	32693	45000	48483
Load (DIANA)	21000	31150	40500	48200	48000
Difference	11 %	22 %	19 %	7 %	-1 %

Tabell 6: Beam 31.1 kN 3-4

Deflection (mm)	2,5	7,5	12,7	17,5	22,9
Loas (TEST)	8674	16500	22907	29800	37141
Load (DIANA)	16458	22000	30246	38500	44925
Difference	47 %	25 %	24 %	23 %	17 %
Load (ANSYS)	8674	16500	22907	29800	37141
Load (DIANA)	18400	26000	34600	40700	40600
Difference	53 %	37 %	34 %	27 %	9 %

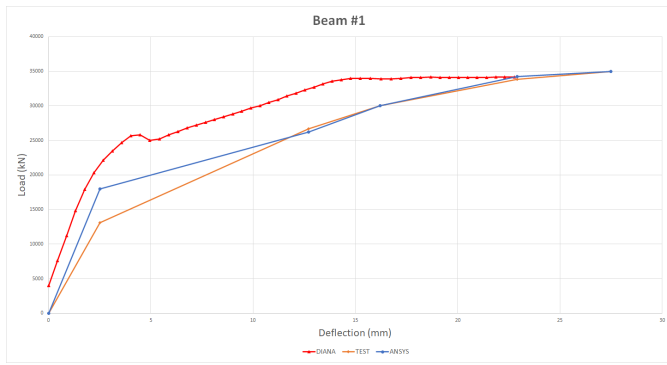


Figure 29: Load deflection for beam 1 with applied prestressing force of 31.1kN

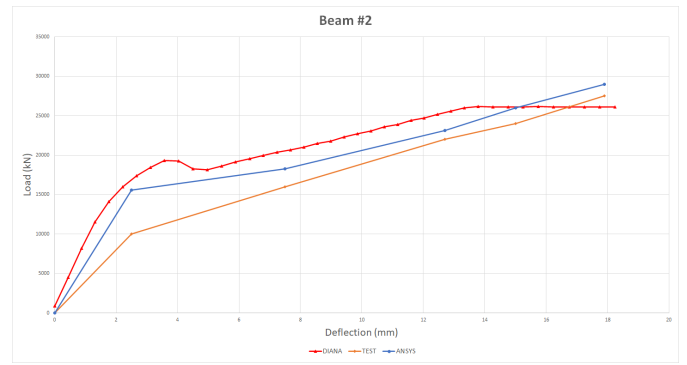


Figure 30: Load deflection for beam 2 with applied prestressing force of 15.6kN

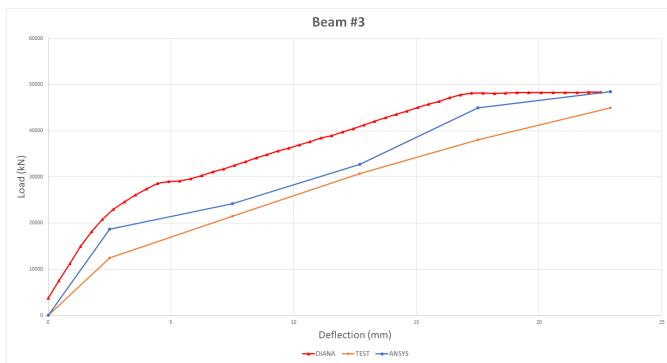


Figure 31: Load deflection for beam 3 with applied prestressing force of 31.1kN

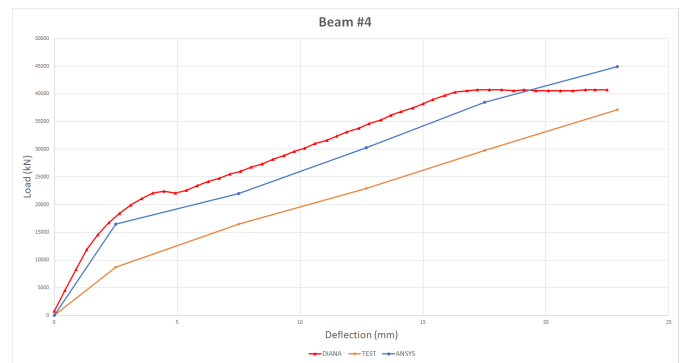


Figure 32: Load deflection for beam 1 with applied prestressing force of 15.6kN

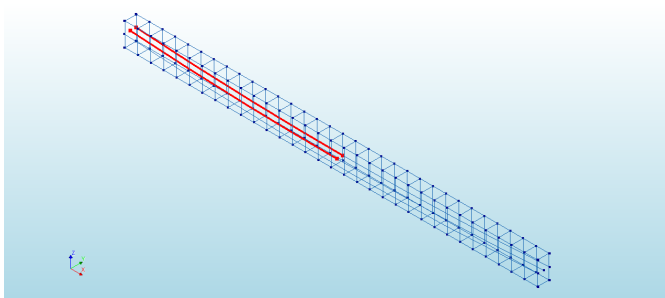
From study following figures can be concluded that the results of the fully prestressing case (31.1 KN) and the partial prestressing force (15.1KN) for post-tensioned concrete beams by comparing it with previous literature study can be considered reliable. The result reveals the response obtained by DIANA for nonlinear analysis are larger but still similar to literature study for given loading condition and deflection.

The difference in the results is due lack of accurate information about concrete properties in publications. Built-in material model for concrete in DIANA can differ significantly from the properties of the concrete that was used for previous tests, as well difference in convergence criteria for nonlinear analysis and mesh density can explain why the behaviour for later loading shows close agreement in deflection than the first load cases.

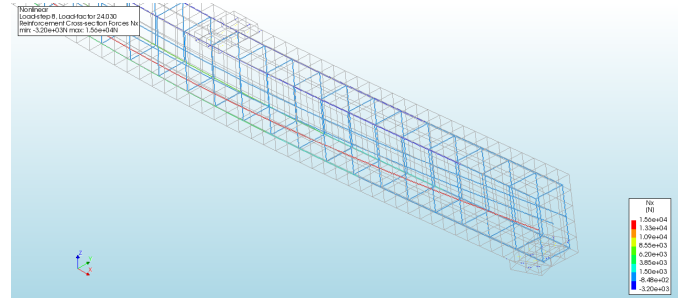
### 8.0.5 Failures in tendons

This part illustrates the procedures of failure analysis of post tensioned concrete beams with broken tendons.

After verifying that the model generated in DIANA is acceptable a new set of beam was modelled. In the next step the post tensioned beam was modelled using the same geometry and material proprieties as the beam before with one addition active reinforcement in the middle of the beam. Same as previous experiments, the load was applied until failure, using hydraulic jacks with an incremental application of deflection of -0.1 mm per step. During experiment has been studies as how damaged tendons affects the overall ultimate limit state as well deflection and the appearance of cracks was measured.

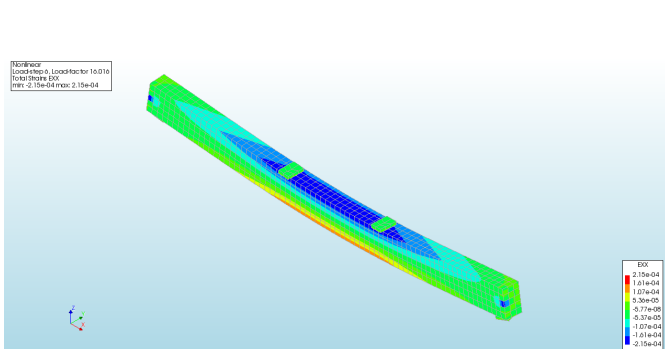


Figur 33: Beam with two damaged tendons

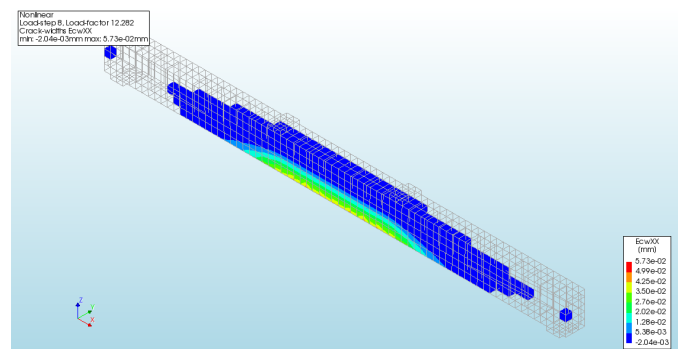


Figur 34: Reinforcement Cross-Section Forces  $N_x$

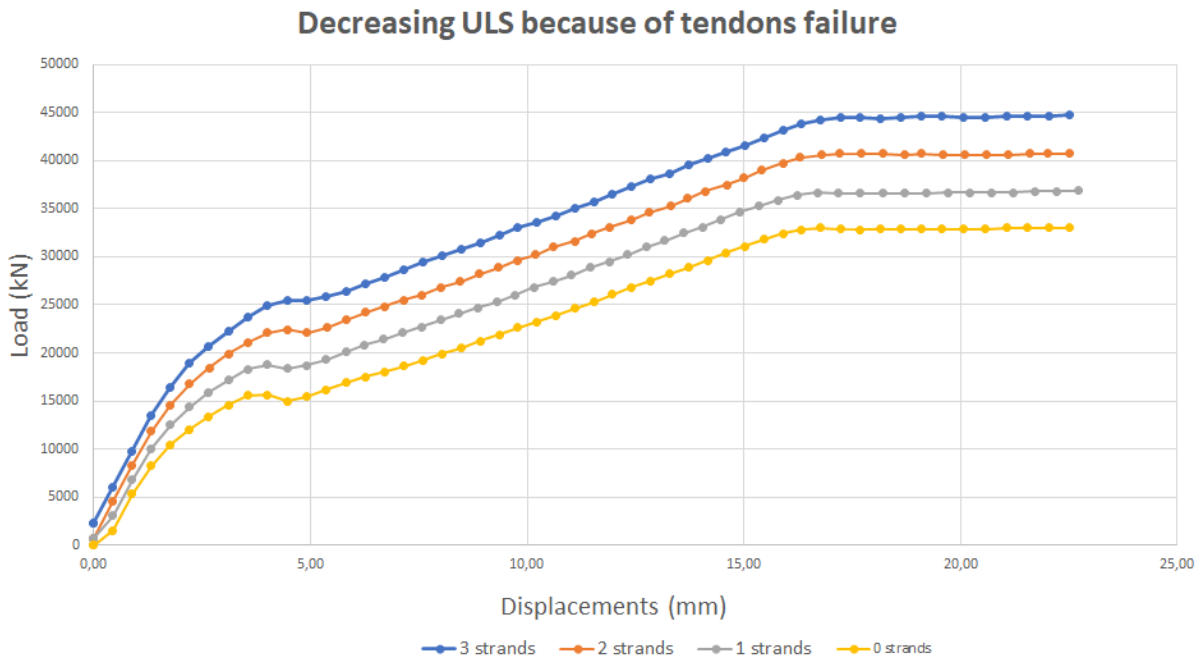
In order for the analysis to be done accurately a series of test have been carried out in which the tendons were gradually damaged. According to "Publikasjon 14" [12] published by the Norwegian Concrete Association, each brokentendon was considered as not existing.



Figur 35: Beam with two damaged tendons

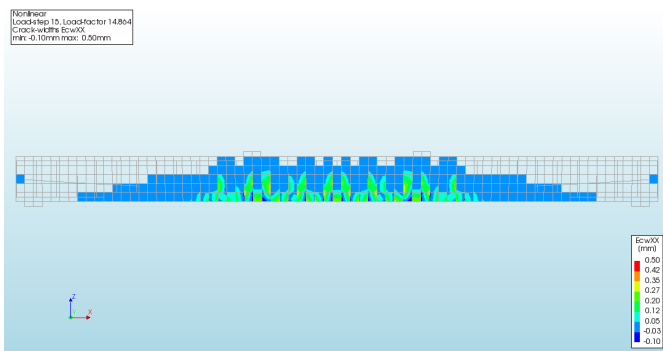


Figur 36: Reinforcement Cross-Section Forces  $N_x$

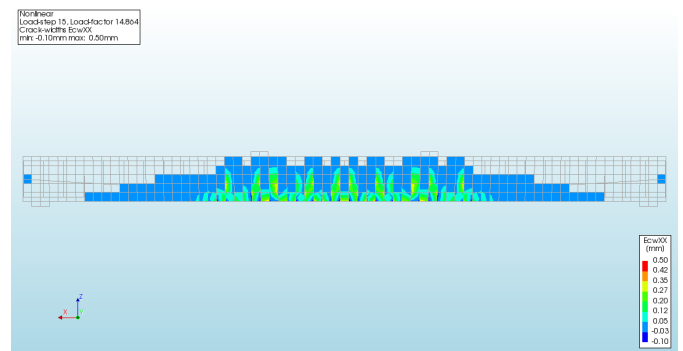


Figur 37: Decreasing of ULS

The parametric study of the ULS for post tensioned beam with one or more damage active reinforcement indicated that there is linear relationship. With each damaged tendon the ULS for beam drops with constant values. The blue line represent situation in which all tendons are active where yellow line show situation in which all tendons are damage.



Figur 38: Cracks on the side where the tendon is located



Figur 39: Cracks on the opposite side of the beam

The analysis shows a slight difference between the cracks in the beam on the side where the tendon is located and on the other side of beam. By using more refined mesh this difference would become more noticeable. From study following figures can be concluded that damage in tendons not only significantly lowers load carrying capacity of beam but also distribution of cracks

---

## 8.1 Parametric study of post-tensioned slab with missing tendons

Slab are one of the most common application of post-tensioning. In order to investigate tendons failure in simple supported post-tension slabs with bonded tendons a series of 3D model were made in DIANA. This chapter contains the methodology for the modelling and analysis of the PT slab. To ensure that the modelling and analysis procedures were representative and valid, models were made with the same geometry and loading procedure as in published experimental results.

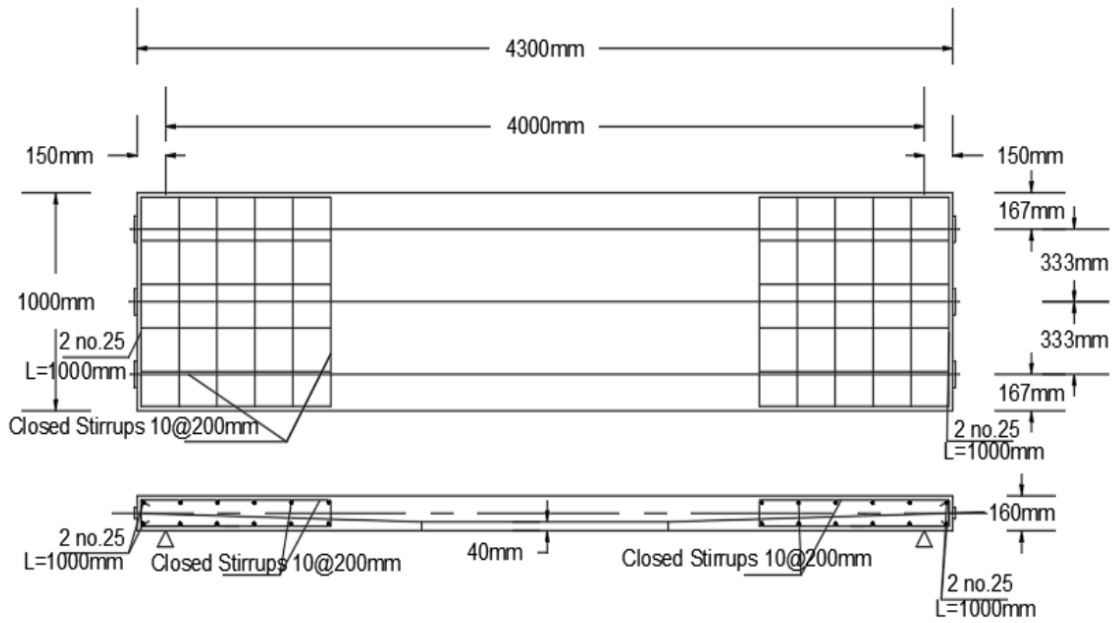
First part present the general modelling method used for all slabs. In the following chapters, the geometry and specific properties of each beam model are presented. The numerical results and the experimental results are compared in the next chapter.

### 8.1.1 Design of PT Slab specimen

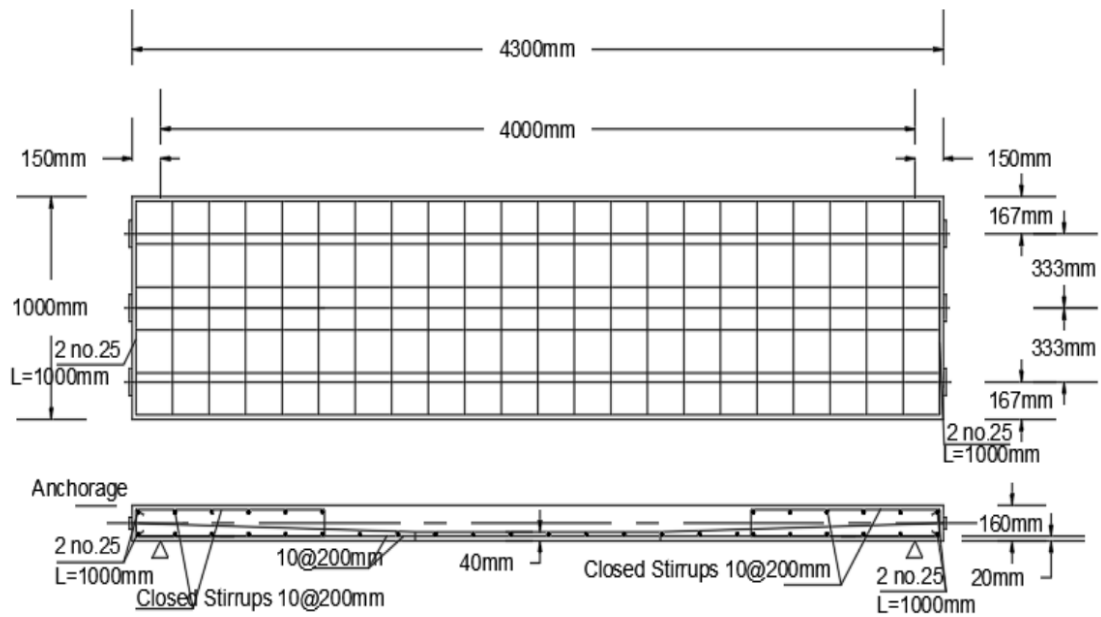
The reference experiments that were used have been found in the research papers described in the following sections. "Prestressed Concrete Slabs with Bonded and Unbonded Tendons" [3] was used as a reference for a non-linear analysis. Article describe research on six simply supported one way slabs: two with bonded tendons, two with unbonded tendons and two with undonded tendons and non-prestressing steel reinforcement are tested in flexure to failure. Because the purpose of the thesis is studying of embedded reinforcement only first part of article was used.

The slab has a total length of 4.300 m, a width of 1.000 m to ensure a span to depth ratio equals 25 a thickness of 0.16m was selected. Each slab contains 3 tendons of a diameter 12.7mm and a concrete cover of 20mm. The tendons are located with spacing 0.333m and with a spacing from the slab edge of 0.167m. Each tendon has one dead end and one live end in terms of the prestressing anchors. Two types of slabs were modeled the geometry, reinforcement, loading, boundary conditions and experimental set-up are presented in figures under. The figures were taken from Jasmin Abdelhalim master thesis [3]





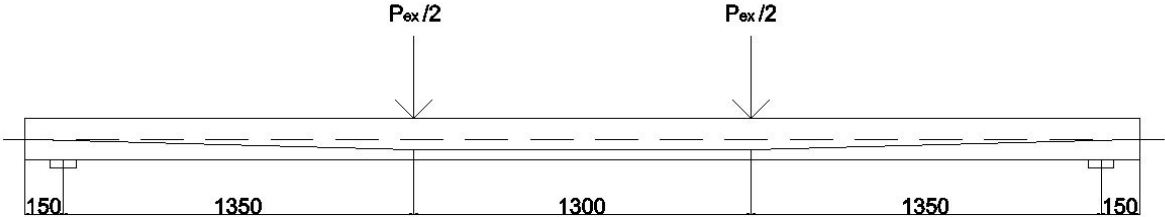
Figur 40: Post-tension bonded slab cross-section and plan with all reinforcement and tendon details



Figur 41: Post-tension bonded slab cross-section and plan with non-prestressing steel reinforcement with all the reinforcement and tendons details

---

All the slab models are simply supported, loaded with a load cell under monotonic loading. The load cell applies a gradually increasing downward load to the beam, as two point loads  $P_{Exp}/2$ . The left support was restrained in all directions (horizontally, vertically and transversely) where right support was restrained only in y and z direction. Steel plates were also used to model load plates between the applied point loads  $P_{Exp}/2$  and the upper edge of the beam. All reinforcement (the longitudinal, shear and post-tensioned) were modelled with a perfect bond between them and the surrounding concrete with other words as embedded reinforcements.



Figur 42: Four-point loading flexural test set-up

Normal weight concrete with compressive strength of 30 MPa at 28 days and tendons with an ultimate strength of 1860 MPa are used for the tested slabs. A doubled-harped tendon shape is chosen with a maximum eccentricity at the slab's mid-span of 40mm and zero eccentricity at the slab ends. The tendon takes an inclined line profile with a length of 1.5m at the slab ends and a straight line profile with a length of 1.30m at the middle part of the span.

Tabell 7: Material properties of the PT slab

<b>Concrete</b>	
Concrete type	Normal weight
Concrete class	C25
Cement type	Normal hardening CE 32.5N
Young's modulus $E$	32009.3
Poisson's ratio $\nu$	0.2
Mean tensile strength $f_{ctm}$	2.56496 $N/mm^2$
Fracture energy in compression $G_c$	34.24 $N/mm$
Crack energy $G_F$	0.136979 $N/mm$
Mass density $\rho$	2.35E-9 $T/mm^3$
<b>Reinforcement steel for strands</b>	
Cross - section	78.5 $mm^2$
Young's modulus $E$	200000 $N/mm^2$
Yielding strength $f_{ym}$	$N/mm^2$
Ultimate strength $f_{um}$	460 $N/mm^2$
Ultimate strain $\varepsilon_{su}$	0.025
<b>Reinforcement steel for PT reinforcement</b>	
Cross - section $\phi$	98.7 $mm^2$
Young's modulus $E$	195000 $N/mm^2$
Yielding strength $f_{ym}$	500 $N/mm^2$
Ultimate strength $f_{um}$	1860 $N/mm^2$
Ultimate strain $\varepsilon_{su}$	0.03
<b>Steel plates</b>	
Young's modulus $E$	210000 $N/mm^2$
Poisson's ratio $\nu$ :	0.3
Mass density $\rho$	0 $T/mm^3$

### 8.1.2 Material models

Modelled was using the same geometry and material properties as the 3D beam referred in part I in this chapter.

### 8.1.3 Numerical iterative procedures

The non-linear analyses for the slab models were executed with the Regular Newton-Raphson iteration method. To ensure a reliable results 20 was selected to be maximum number of iteration. Energy convergence criterion was chosen as convergence norm with 0.005 tolerance and 10000 abort criterion. All others settings remains on default setting.

---

#### 8.1.4 Modeling of 3D slab

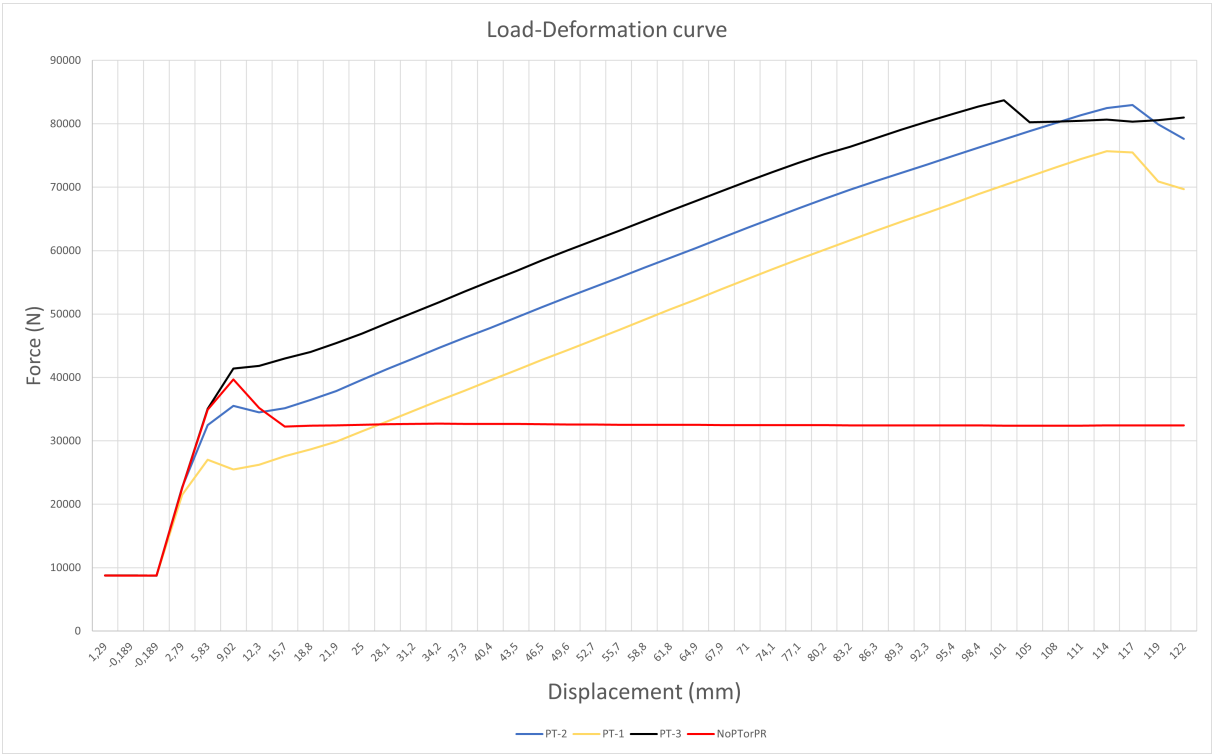
Similarly to the 3D PT beam, the slab was subjected to two point loads applied symmetrically about midspan until the beam reached failure. Based on "Guidelines for Nonlinear Finite Element Analysis of Concrete Structures" [11] the minimum element size should be  $\frac{h}{6}$ , or 27mm. An attempt of running a general analysis on the slab model was made with an element size of 25 mm. Because analysis was too timeconsuming it was concluded to made mesh with an element size of 50mm. Though time shortened it was still too timeconsuming at the end an adaptive mesh was made with an element size of 75mm.

### 8.1.5 Results

#### Displacement :

The resulting load-deflection curve from the nonlinear analysis of the PT slab is presented in figure below. The results of analysis show similar curves as for PT beam in the previous chapter that is why, similar conclusions can be drawn. Load carrying capacity of a slab diminishing with each failed tendons, the parametric study shows that the relationship between load carrying capacity and deflection is linear.

The red line represent slab without any passive reinforcement beside two steel cages located at the ends of the beam. [look Figure 37] Failure was sudden and did not provided any warning in other words it was brittle failure. The results obtained from the nonlinear analysis differ from publication "Prestressed Concrete Slab with Bonded and Unbonded Tendons" [3] and are exactly ten times smaller. The values Jasmin obtained in her master thesis seems unreliable. It is hard to expect a slab without any longitudinal and shear reinforcement can have similar performance as full reinforced slab.



Figur 43: Load-Deformation curve for data collected from DIANA located at mid-span

## Crack widths :

Figures shows cracks patterns at the time of failure for each slabs. As an adaptive mesh was made with an element size of 75m which is three times more then recommended this affected the readability of the results especially crack widths. It may be concluded that the slab without one active tendon in the middle ends up with more shallow cracks which are more scattered across bottom compered to slab with three working tendons.

Forth figure shows crack width for beam with only one working tendons that is located at the left side of the slab. Because the slab is tilted 90 degrees the part of the slab where the active tendon is still active is at the bottom of the figure. More cracks formed on the opposite side to the active tendon.

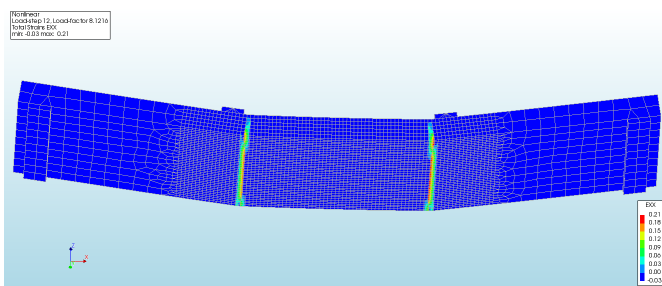


Figure 44: Crack widths for a beam without passive reinforcements

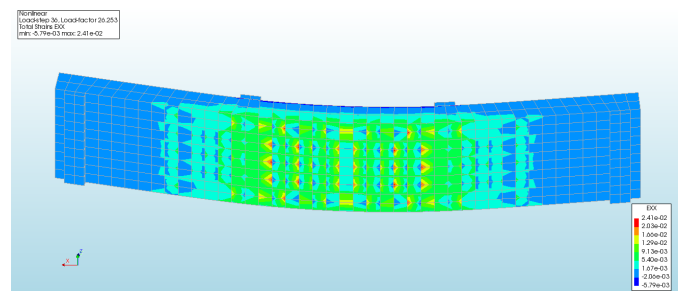


Figure 45: Crack widths for beam with three working tendons

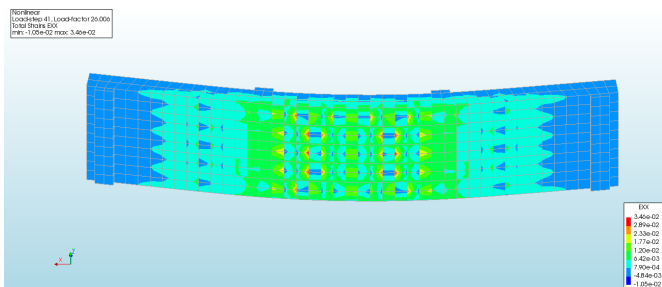


Figure 46: Crack widths for beam with one broken tendon

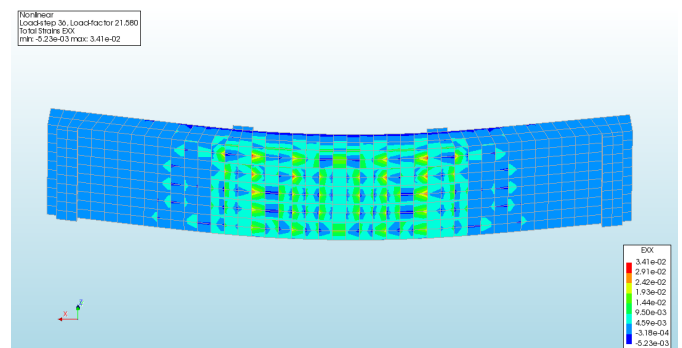


Figure 47: Crack widths for beam with two broken tendons

Even after selecting a element size of 25 mm for the most vulnerable parts of the slab to cracking no significant increase in slab strength was observed. The maximum displacement increased from 8.2mm for 12.1mm however, this values is still much lower then max displacement for slab with non-prestressing steel reinforcement.

---

## 9 Sykkylvsbrua

### 9.1 General information

The Sykkylven Bridge (Norwegian: Sykkylvsbrua) is a concrete bridge that crosses the Sykkylvsfjorden in Sykkylven Municipality in Møre og Romsdal county, Norway. It connects the municipal center of Aure with the village of Ikornnes on the other side of the fjord. Sykkylvsbrua is a 22 years old bridge with one lanes and is a part of the Fv 5914 route (Old Fv 71). The bridge has a length of 860 m, distributed over fifteen spans with a maximum length of 60 meters.

In the following chapters, the modelling approach of the bridge is described and the results from the analysis are presented. Similarly to Part I, a parametric study was performed to investigate the structural effects of damage in active reinforcement on the performance of concrete box girder bride. The nonlinear behaviour of the bridge has been studied by applying the self weight and gradually increasing vertical traffic loads until the bridge failure.



Figur 48: Sykkylvsbrua

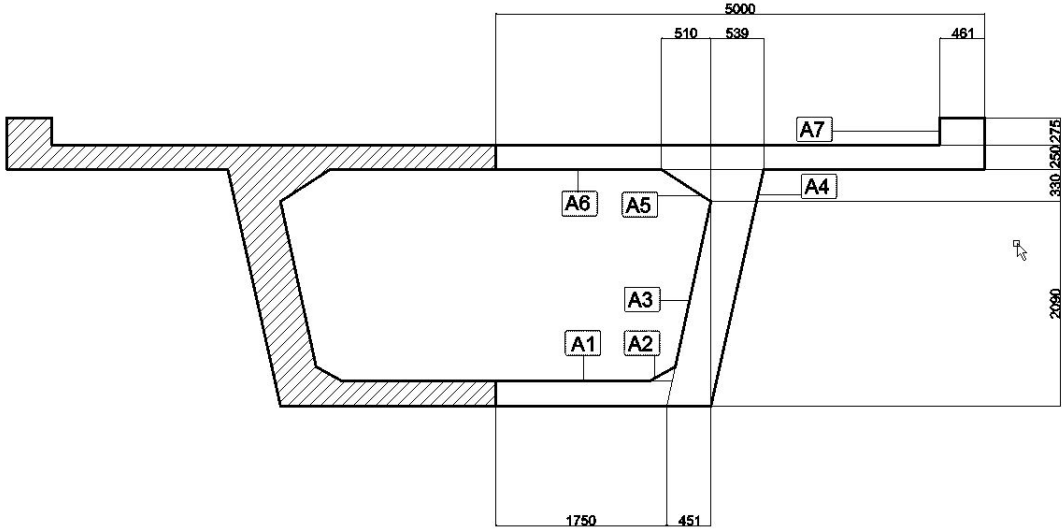
## 9.2 Modelling of the post-tensioned beam bridge

It have to be said that no information of the materials or tests was done over the bridge, model was based on information prescribed in the construction model project. Due to the complexity and size of the bridge, only half of span has been modeled.

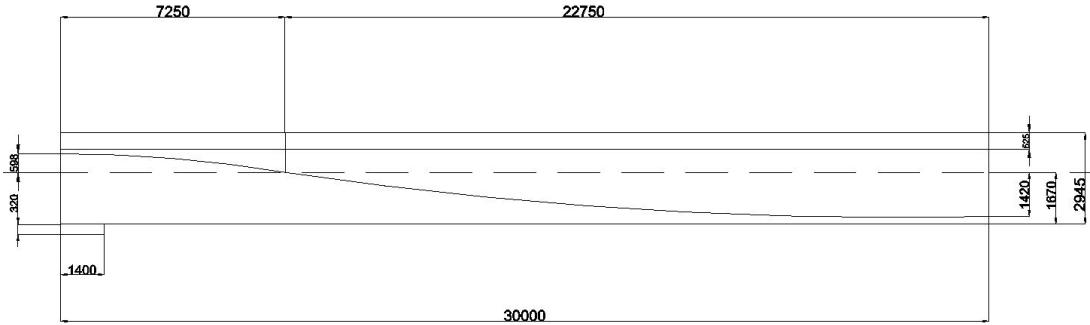
### 9.2.1 Bridge cross section

The bridge is built up with a box girders with a constant height. Spans lengths varies between 58m to 60m. The bridge model was idealized thanks to the simplification of its geometry. Calculation shows in Appendix give following results

- Cross section:  $A = 6.21 \cdot 10^6 mm^2$
- Neutral axis:  $z_c = 1670mm$
- Second moment of area:  $I_y = 6.36 \cdot 10^{12} mm^4$



Figur 49: Cross section of box girder



Figur 50: Neutral axis



---

### 9.2.2 Bridge reinforcements

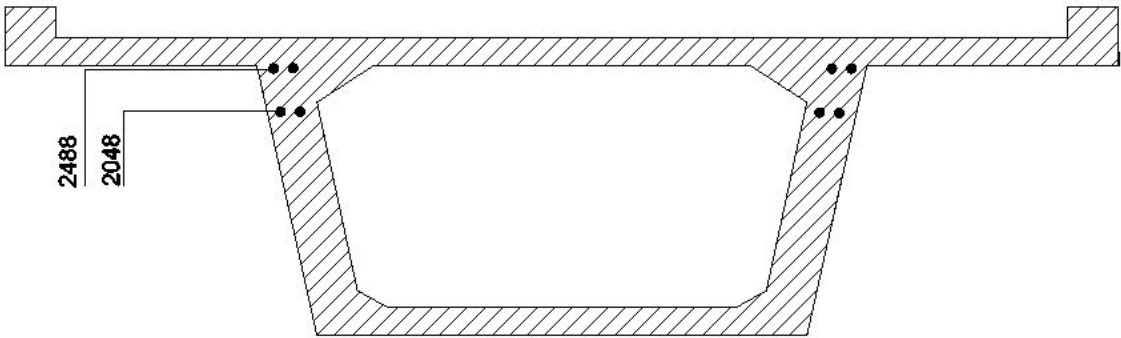
The bridge consists of concrete as well as longitudinal, transverse and prestressing reinforcement. In addition, it has asphalt as a coating and railings of different steel profiles. As the main purpose of this thesis was to investigate the damage in simply supported box girder bridge asphalt as well as railings were not been considered in the analysis because of both have negligible influence on the performance of the bridge.

All types of bridge model reinforcements were made as smililarly to the reinforcement on Sykkylsbrua following the technical drawings provided by Staten Vegvessen. The model is mainly based on drawings attached to the end of this document. Both passive and active reinforcement was modelled as embedded reinforcements.

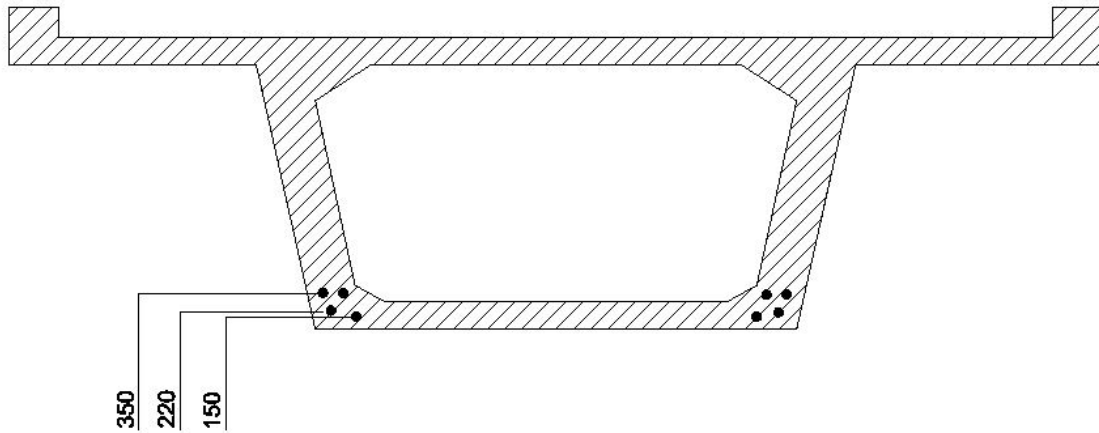
Passive reinforcements of bridge consist of  $\phi 12, \phi 16, 16$  and  $\phi 25$  steel bars located where it is necessary and according to the cover requirements for the various construction parts. The passive reinforcement in the bridge has a function such as tensile reinforcement, pressure reinforcement and shear reinforcement.

The Sykkylsbrua has eighth tendons that have a parabolic shape and so the eccentricity  $e$ , varies along the length of the beam as presented in figure 49 .The maximum eccentricities for upper tendons were  $e_1 = 2312$  mm at midspan and  $e_2 = 350$  mm over the support and the maximum eccentricities for lower tendons were  $e_1 = 1872$  mm at midspan and  $e_2 = 150$  mm . Distance between upper tendon and lower were at midspan was 200 mm and 440 mm over midspan

Following the technical drawings a concrete cover for upper and lower part of box girder was set to  $60 \pm 5$ mm and  $60 \pm 5$ mm for the inside a concrete cover was set to  $45 \pm 5$ mm



Figur 51: Placement of prestressing reinforcement at support

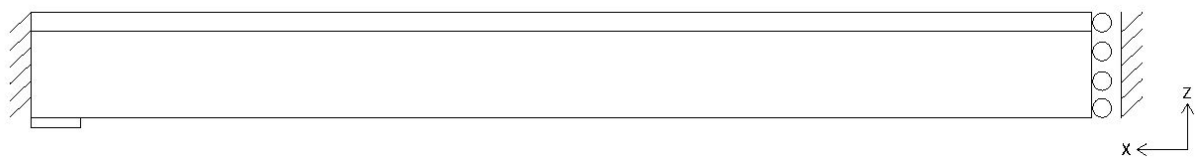


Figur 52: Placement of prestressing reinforcement at midspan

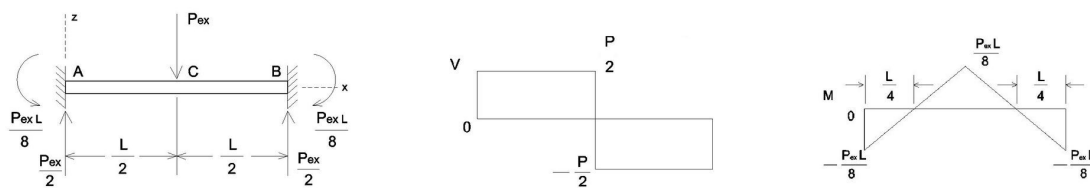
### 9.3 Boundary conditions and constraints

Box girder is fixed at the left end, while the center part is held against rotation (y and z-axis) and displacement in the transverse direction. In the longitudinal and vertical directions, mid span is free to move. To simulate the continuation of the bridge concrete edge over support is fixed in x-direction. The support plate under box girder is given fixed support by holding all nodes in this surface against displacement in the y and z directions. With these selected boundary conditions, it is assumed that the model simulates the behavior of a main span on Sykkylvsbrua to a good enough degree. Still, there will be some sources of error in them selected boundary conditions

Figure under show selected boundary conditions for the numerical model



Figur 53: Box girder boundary conditions



Figur 54: Statically Indeterminate Beam

---

## 9.4 Material properties of the bridge model

### 9.4.1 Loads

Loads were selected according to N400 and divided by their variation over time as follows:

- Permanent load: Self-load
- Variable load: Traffic load and wind load
- Random load: Collision, fire etc.

Only self-load, traffic load and prestressing reinforcement force are taken into accounting the analysis.

### 9.4.2 Self weight

Concrete self-weight was calculated from the average cross-section of the box girder multiply by characteristic dead weight for concrete  $g_c = 25kN/m$ . The self weight was found to be  $g = 149kN/m$  Calculations can be found in the attachments.

$$g = g_c \cdot A$$

### 9.4.3 Traffic loads

Traffic loads according R412 are defined as as the loading in the vertical and the horizontal direction from road traffic, consisting of cars, trailers and special vehicles such as industrial transport as well pedestrians. Calculations of traffic loads have been made accordingly to NS-EN 1991-2: 2003 + NA: 2010 - Eurocode 1: Loads on structures Part 2: Traffic load on bridges [cytat], hereinafter referred to as EK1-2

#### Serviceability class

Ensuring serviceability is central to the design of bridges. A structure shall be designed and executed in such a way that it will, during its intended life with appropriate degrees of reliability and in an economic way. Each bridge has a serviceability class that reflect type of load that can cross the bridge without restriction. According to R412 there are four serviceability classes (Bk10), (BkT8), (Bk8) and (Bk6).Rossvollbrua has a serviceability class of Bk10/50.[13] For bridges designed in accordance with the load regulations of 1969 and later, it is not necessary to make classification, as all can withstand Bk 10/50 . The exception is ferry quays with span  $L \leq 11.5m$  and  $L \geq 15.0m$ .[14]

In Bk10/50, each vehicle can apply a maximum load of 10 tons per axle and a total of 50 tons.

Carriageway width $w$	Number of notional lanes	Width of a notional lane $w_l$	Width of the remaining area
$w < 5,4 \text{ m}$	$n_l = 1$	3 m	$w - 3 \text{ m}$
$5,4 \text{ m} \leq w < 6 \text{ m}$	$n_l = 2$	$\frac{w}{2}$	0
$6 \text{ m} \leq w$	$n_l = \text{Int}\left(\frac{w}{3}\right)$	3 m	$w - 3 \times n_l$

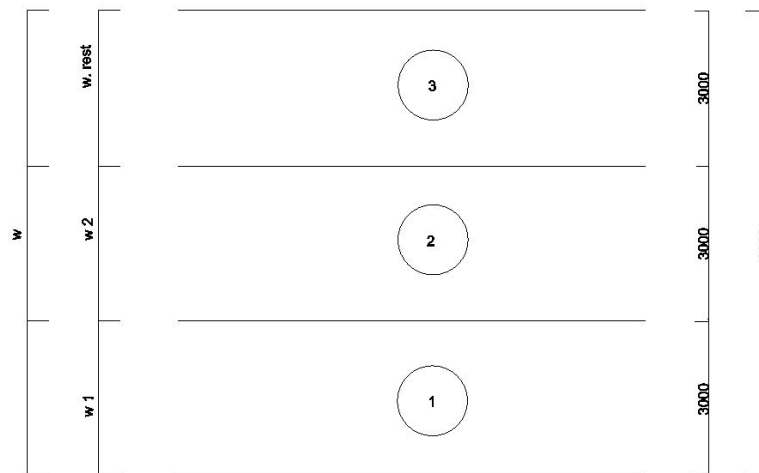
NOTE For example, for a carriageway width equal to 11 m,  $= \text{Int}\left(\frac{w}{3}\right) = 3$ , and the width of the remaining area is  $11 - 3 \times 3 = 2 \text{ m}$ .

Figur 55: Table 4.1 EK1-2 The number of notional lanes for carriageways

### Notional lanes

The number of notional lanes for carriageways was found accordingly to Table 4.1 EK1-2. Sykkylsbrua has a carriageway of  $w = 9\text{m}$  this is why the integer number of notional lanes is equal to 3. There will be two theoretical notional lane  $w_1 = w_2 = 3\text{m}$  and a remaining part  $w_{rest} = 2.5\text{m}$

The roadway model looks like this:



Figur 56: The model of notional lanes for carriageways

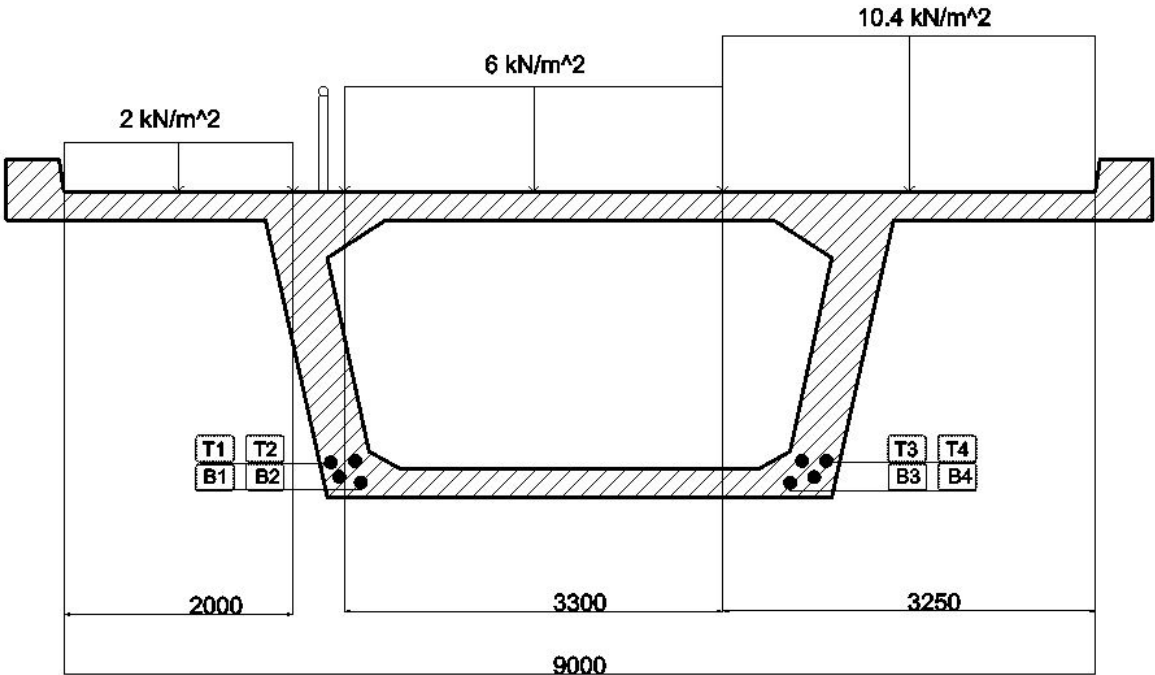
Such a theoretical division of the carriageway is close to the real division of the road, where  $w_1 = 3.3\text{m}$ ,  $w_2 = 3.25\text{m}$  and  $w_{rest} = 2.45\text{m}$

---

### Load combinations

Four different load models are defined in EK1-2:

- Load model 1 (LM1): The model consists of normal distributed load and one bogie load per theoretical roadway. This model is used for general and local verification.
- Load model 2 (LM2): The model consists of a single axle load, which can be placed where it will be most unfavorable load effect. This model is used to simulate heavy vehicles.
- Load model 3 (LM3): The model consists of a collection of axle loads and takes into account special vehicles. This model is used for general and local verification.
- Load model 4 (LM4): The model consists of loads from pedestrians in large groups. This model is used in or near cities. The application for this model is for general verification only.



Figur 57: Load combination and reinforcement numbering

---

#### 9.4.4 Prestressing force

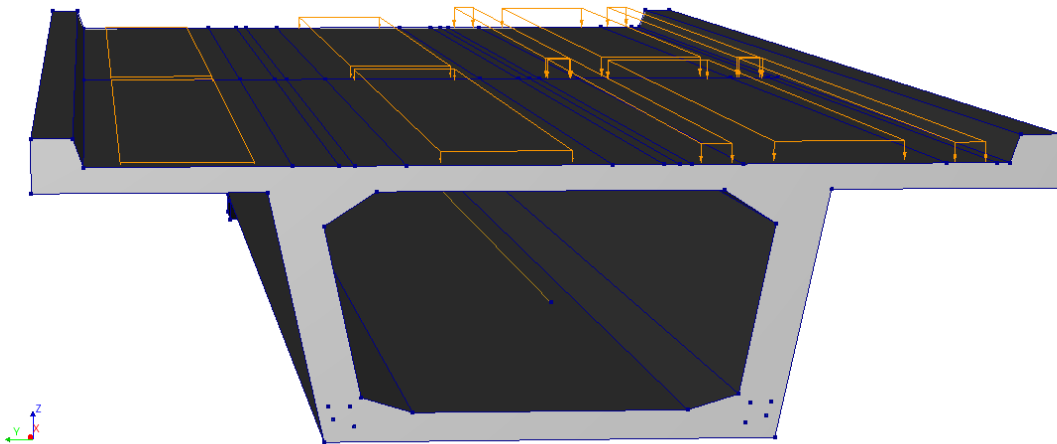
Sykkylvsbrua has eight post tensioned tendons, four on each side of box girder at 2 heights. The tendons are made of multiply strands. The area per strands is 140 mm<sup>2</sup> as give area per cable  $A_p = 1680 \text{ mm}^2$

The post tensioned tendons have a characteristic tensile strength  $f_{pk}=1860\text{N/mm}^2$  and a characteristic 0.2% yield strength  $f_{p0.1k} = 1670\text{N/mm}^2$  In standard EK2 the prestressing force is defined as:

$$P_{max} = A_p \cdot \sigma_{p,max} \quad \text{where} \quad \sigma_{p,max} = \min(0,8f_{pk}; 0,9f_{p0.1k})$$

Technical drawings for Sykkylvsbrua claim that the prestressing force for each tendon is  $S_{0.2=P_{max}} = 2536\text{kN}$ . This force is calculated as follows:

$$S = 0,8 \cdot S_{0,2}$$



Figur 58: 3D model with load combination

## 9.4.5 Material properties of the bridge model

Tabell 8: Material properties of the box girder

<b>Concrete</b>	
Young's modulus $E$ :	38000 $N/mm^2$
Poisson's ratio $\nu$ :	0.2
Compressive strength $f_{cm}$ :	31.17 $N/mm^2$
Tensile strength $f_{tm}$ :	4.35 $N/mm^2$
Compressive fracture energy $G_c$	34 $N/mm$
Mode - I tensile fracture energy $G_F$	0.136 $N/mm$
Mass density $\rho$	2.4E-9 $T/mm^3$
<b>Reinforcement steel for strands</b>	
1.Diameter $\phi 12$	12.0 $mm$
2.Diameter $\phi 16$	16.0 $mm$
3.Diameter $\phi 20$	20.0 $mm$
4.Diameter $\phi 25$	25.0 $mm$
Young's modulus $E$	200000 $N/mm^2$
Yielding strength $f_{ym}$	434.8 $N/mm^2$
Ultimate strength $f_{um}$	521.7 $N/mm^2$
Ultimate strain $\varepsilon_{su}$	0.075
<b>Reinforcement steel for PT reinforcement</b>	
Cross-section $\phi$	1680 $mm$
Young's modulus $E$	1950 $N/mm^2$
Yielding strength $f_{ym}$	1426 $N/mm^2$
Ultimate strength $f_{um}$	1466 $N/mm^2$
Ultimate strain $\varepsilon_{su}$	0.014
<b>Steel plates</b>	
Young's modulus $E$	210000 $N/mm^2$
Poisson's ratio $\nu$ :	0.3
Mass density $\rho$	0 $T/mm^3$

---

## 9.5 Material models

In the following section are presented properties assignee to material models.

### Concrete

---

When defining the properties for the concrete slab, the Element Class was set to Structural Solids. The concrete material was defined with the properties stated below.

Class:	Concrete and masonry
Material model:	Total strain based crack model
Crack orientation:	Rotating
Tensile curve:	Exponential
Crack bandwidth specification:	Rots
Poisson's ratio reduction model:	No reduction
Compression curve:	Parabolic
Reduction due to lateral cracking:	Reduction model by Vecchio and Collins 1993
Lower bound reduction curve:	0,6
Stress confinement model:	No increase

### Steel plates

---

The steel plate has a total length of 0.150m, a width of 1.000 m and a thickness of 0.350m was selected. Load plates and support plates were defined as.

Class:	Steel
Material model:	Linear elastic isotropic
Elastic modulus:	210000 $N/mm^2$
Poisson's ratio $\nu$ :	0.3
Mass density:	0

### Reinforcement

---

The passive reinforcements of the slab models, including the tendons and stirrups as well active reinforcements, were defined as.

Class:	Reinforcements
Material model:	Von Mises Plasticity
Plastic hardening :	Plastic-strain-yield stress
Hardening hypothesis:	Strain hardening
Haredning type :	Isotropic hardening

Strain-Stress diagram for prestressed reinforcement was defined as Total strain-stiffness ratio. Therefore it differs from the others figures.



## Interface material properties

Surface between slab and steel plates were defined as.

Class:	Interface elements
Material model:	Nonlinear elasticity
Type:	2D line interface
Normal stiffness modulus-y:	34200 $N/mm^3$
Shear stiffness modulus-x:	0,000342 $N/mm^3$
No-tension or diagram:	Notension with shear stiffness reduction
Critical interface opening for reduction:	0,001 $mm$
Normal/shear stiffness reduction factor:	0

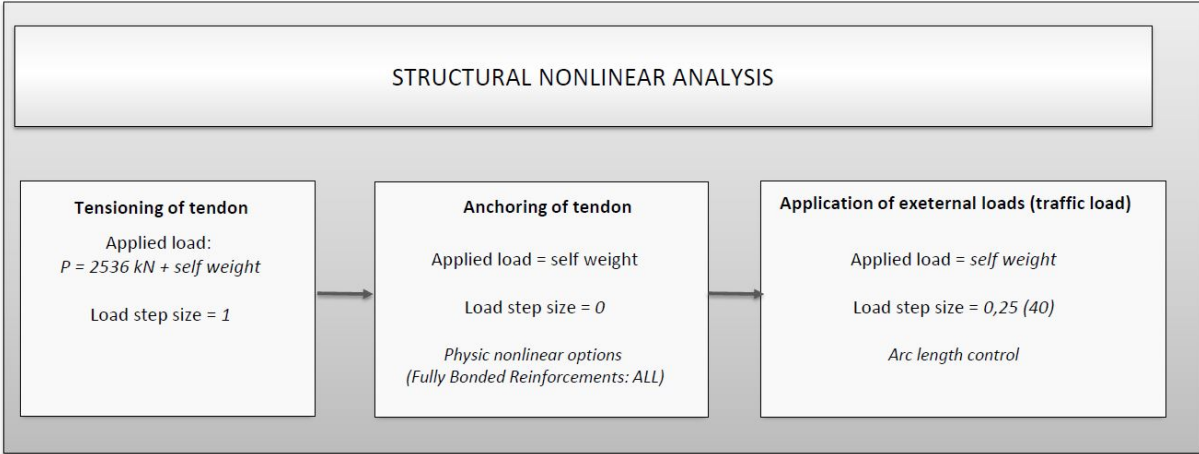
### 9.5.1 Numerical iterative procedures

The non-linear analyses for the slab models were executed with the Regular Newton-Raphson iteration method. To ensure a reliable results 20 was selected to be maximum number of iteration. Energy convergence criterion was chosen as convergence norm with 0.001 tolerance and 10000 abort criterion. All others settings remains on default setting.

## 9.6 Meshing and analysis of the bridge model

Following "Guidelines for Nonlinear Finite Element Analysis of Concrete Structures" [11] the minimum element size should be  $\frac{h}{6}$ , or 460 mm. An adaptive mesh was made with an element size of 300 mm.

To study the nonlinear behaviour of the bridge, a nonlinear analysis was performed with gradually increasing traffic load until failure. Figure under visualises the analysis setup in DIANA for the embedded model.



Figur 59: Analysis of the bridge model

# 10 Results from bridge model analysis

## 10.1 Deflection

Bridge deflection serviceability limitation under the vehicle load effect is a condition to control the deflection of a bridge without causing severe damages. With the established probability model of the extreme load effect, structural serviceability reliability can be estimated with a predefined deflection limit.[15] Several design specifications have defined the limit deflection of multiple bridges. These criteria are summarized in table below:

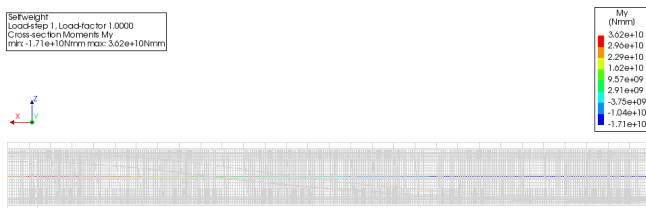
Tabell 9: Bridge deflection limits

Bridge types	Materials of the bridge girders	Deflection limits
Simply supported bridges	Concrete or steel	L/800
Cantilever bridge	Concrete or steel	L/300
Cable-stayed bridges	Concrete	L/500
	Steel	L/400
Suspension bridges	Steel	L/350

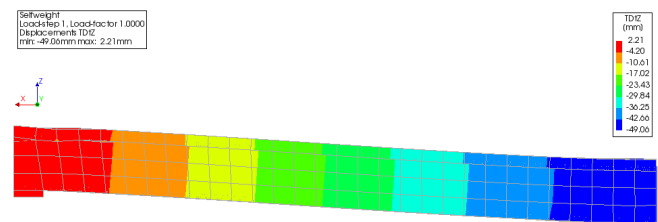
Note:  $L$  is the bridge span length

In accordance with the standards bridge deflection serviceability is 75mm the analyzes in the program confirm this as the main cracks occur when the bridge deflection is higher than 75mm.

A series of two control tests has been carried out to detected potential errors before the loads were combined and the nonlinear behaviour was studied. In test nr.1 only self weight was applied and in test nr.2 was tested the response of the bridge with only the prestressing load.The results are compared to the analytical calculations that can be found in Section E of the Appendix.



Figur 60: Moment when only self weight is applied



Figur 61: Deflection when only self weight is applied

The bending moment over the support according to DIANA is 36 200kN and -17 100kN at support. It means that results are 8% higher at support and 2% at midspan then analytical calculation. The difference between the analytical and experimental loads for the box girder was less than 10%, confirming the analytical calculations and the carried experimental program accuracy.

Tabell 10: Analytical results for the bridge loaded with self weight and traffic load

	Force P/2 [kN]	$M_{support}$ [kNm]	$M_{midspan}$ [kNm]	Deflection [mm]
Self weight g	4 470	33 525	- 16 763	41,7
Traffic load q	1 416	-10 620	5 310	13,2

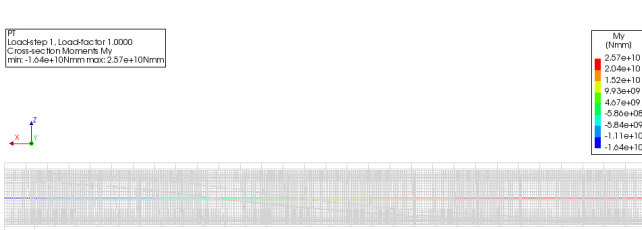


Figure 62: Moment when only PT is applied

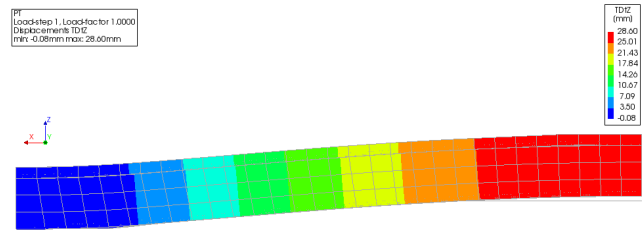


Figure 63: Deflection when only PT is applied

Tabell 11: Analytical results for the bridge loaded with prestressing load

	Moment at support [kNm]	Moment at midspan [kNm]	Deflection [mm]
Load q1	-33 390	16 695	31.0
Load q2	13 292	0	0
Total	-20 098	16 695	31.0

The bending moment over the support according to DIANA is 25 700kN and -16 400kN at support when only PT is applied. The difference between the results is much larger than in the previous example. 20% for moment at support and 1.7% at midspan. The difference between the results may be due to the fact that in this test much larger element size was used which could affect the accuracy of the measurements.

As presented in Table under, the results from DIANA analysis and the analytical calculations are generally in good agreement.

	Deflection (pt) [mm]	Deflection (sw) [mm]	Deflection (tl) [mm]
DIANA	28.6	47,9	8.36
Analytical calculations	31.0	41.7	10.7
Difference	+7.7%	-13.9%	+21%

A series of fifteen tests has been carried out. In each test, a different combination of tendons was removed from box girder. The table below presents a detailed description of the name of the test, the number of active reinforcements removed, and the position in which the reinforcement was located. In the leftmost column there are 8 dots representing 8 prestress reinforcement, the black dot means that the tendon is working and a force of 2563kN is applied on it, the white dot mean that the tendons is broken and no force is acting on it.

Abbreviated form of the sample name description :

- **BGMT**: *Box Girder with Multiplie Tendons*
- **BGS**: *Box Girder with Symmetrical removed Tendons*
- **BGWT**: *Box Girder Without Tendons*
- **BGL** or **BGR**: *Box Girder with removed tendons on the Left or Right side*

Test nr	Specimen Name	Number of tendons	Broken tendons		
1	BGMT	8	0	●●●●	●●●●
2	BGS1	6	T2,T3	●●○●	○●●●
3	BGS2	6	B2,B3	●●●○	●●●○
4	BGS3	4	T2,T3,B2,B3	●●○●	○●○●
5	BGS4	4	T1-T4	○●○●	○●○●
6	BGS5	4	B1-B4	●●○●	○●○●
7	BGS6	2	T2,T3,B1-B4	○●○●	○●○●
8	BGS7	2	T1-T4,B1,B4	○●○●	○●○●
9	BGUT	0	T1-T4,B1-B4	○●○●	○●○●
10	BGL1	7	T1	●●●●	●●●●
11	BGL2	5	T1,T2,B1	○●○●	●●●●
12	BGL3	4	T1-T2,B1-B2	○●○●	●●●●
13	BGR1	7	T4	●●●●	○●○●
14	BGR2	5	T3,T4,B4	●●●●	○●○●
15	BGR3	4	T3-T4,B3-B4	●●●●	○●○●

Figur 64: Analysis of the bridge model

Tabell 12: Results 1

Specimen Name	Initial deflection (mm)	Maximum Deflection (mm)	Experimental load at failure (kN)
BGMT	5,0	102,0	20983,0
BGS1	9,3	97,3	18927,4
BGS2	8,7	96,8	19628,3
BGS3	19,7	98,3	17949,8
BGS4	22,6	99,6	17689,1
BGS5	18,4	99,2	18113,6
BGS6	37,4	92,2	16964,9
BGS7	40,6	102,0	17410,0
BGUT	49,9	110,0	16929,3
BGL1	7,1	91,5	18648,4
BGL2	16,7	93,6	18092,1
BGL3	22,1	98,6	18312,8
BGR1	7,1	87,7	18425,7
BGR2	16,8	99,8	18148,6
BGR3	20,4	101,3	17927,3

Tabell 13: Results 2

Specimen Name	Initial deflectin (%)	Deflection at midspan (%)	Load capacity reduction (%)
BGMT	-	-	-
BGS1	84,9 %	-4,6 %	-10 %
BGS2	73,0 %	-5,1 %	-6 %
BGS3	291,7 %	-3,6 %	-14 %
BGS4	349,3 %	-2,4 %	-16 %
BGS5	265,8 %	-2,7 %	-14 %
BGS6	643,5 %	-9,6 %	-19 %
BGS7	707,2 %	0,0 %	-17 %
BGUT	892,0 %	7,8 %	-19 %
BGL1	41,2 %	-10,3 %	-11 %
BGL2	232,0 %	-8,2 %	-14 %
BGL3	339,4 %	-3,3 %	-13 %
BGR1	41,9 %	-14,0 %	-12 %
BGR2	234,0 %	-2,2 %	-14 %
BGR3	305,6 %	-0,7 %	-15 %

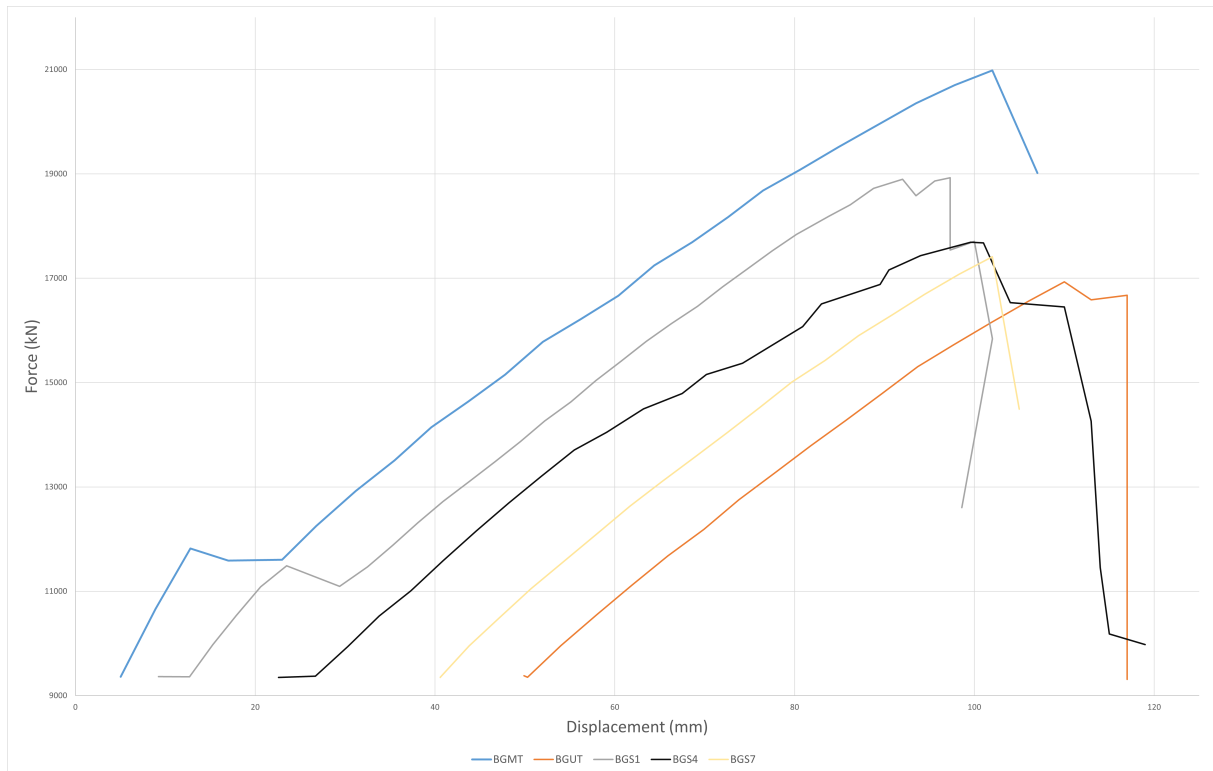


Figure 65: Load-Deformation curve for some of the tests

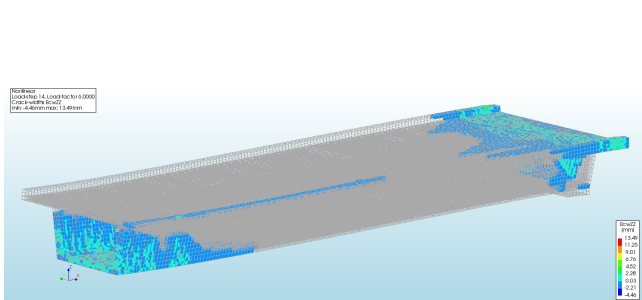
Graph above shows the reaction force versus displacement for one 60 meter span. The design traffic load of the bridge according to standard is 1 416kN or 2 832kN for full span. Load due self weigh is 4 470kN or 8 940kN. As presented in the graph above the size of the loads is about 4.5 times higher for **BGMT** than the design traffic load of the bridge. When all prestressing reinforcement are broken (**BGUT** case) the maximum load capacity for box girder drops from 20 983kN to 16 929kn, around 21%. It still allows the bridge to withstand almost three times greater load then the design traffic load.

As presented in diagram over, the results from DIANA are similar to those from the Part I when a simple supported beam was tested. To make the diagram as clear as possible, only some of the fifteen tests are presented. From resultants can be concluded that there is a linear correlation between bridge load capacity and numbers of tendons. It is logical that the less active reinforcement is working the less weight the bridge can withstand.

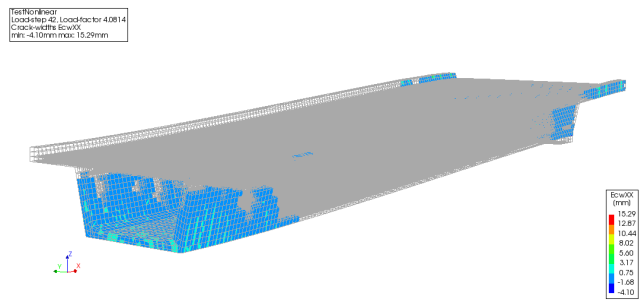
---

### 10.1.1 Concrete Cracks Patterns

Some steps have been taken towards analysis concrete crack patterns but insufficient time combine with too weak computer to be able to do a thorough analysis resulted in only some of the planned tests being carried out. Map of the cracks on the both sides of the structure look very similar to each other. Above have been presented results for box girder with eight PT reinforcement and box girder with only PT reinforcement on left side. An adaptive mesh was made with an element size of 200 mm however, this was not enough to make the results clear.



Figur 66: BGMT



Figur 67: BGR3

---

## 11 Summary

This section will draw the main conclusions from the work done in this thesis and some suggestions for further study are presented

### 11.1 Commentary

This thesis has dealt with how damages in embedded active reinforcements affects concrete structures. A numerical models have been created to simulate damages in post-tensioned concrete beams and box girder. The models have been verified against parametric results but there are some uncertainty associated with how good the models are reflects reality and whether the results are valid.

The beam models in first part of the thesis were created with the intention of recreating the experimental results that were reported in three research papers. Lack of information as well possibility of misinterpreting the method and results could have influenced the test and explain some of the difference in results. This was mainly observed for the slab model without passive reinforcement where the crack occurred much earlier than in the data provided in the research paper.

For the second part of this thesis, half span of Sykkylvsbrua was modelled and loaded with self weight and traffic load in addition to the post tensioning load. Despite the fact that this model was simplified it can be assumed that results are somewhat representative. For box girder model match between numerical results and the analytical results were satisfactory. As previously discussed, the beam model as well box girder modelled display the same behaviour when some of the active reinforcement was damaged.

### 11.2 Conclusion

In this thesis, a post-tensioned beam in two and three dimension and a span of a post-tensioned beam bridge were successfully modelled. The numerical results were overall reasonable when compared to analytical and experimental results.

By using a different combination of broken tendons in structure it was possible to study the what kind of structural effects it have on system. The results from simulations in this thesis show that number broken of reinforcement and is position have an impact on the ULS of the structure.

Results linked to the Sykkylvsbrua bridge show that the structure is well equipped for damage in post tensioned reinforcement. Even if all active reinforcement are broken, the



---

bridge will withstand the design traffic load. For crack analysis the most critical area for bridge is found to be near support and at the lower part of box girder at the mid span

The difference between the analytical and experimental loads for the box girder was less than 15% for most of compare, confirming the analytical calculations and the carried experimental program accuracy.

### **11.3 Future work**

During the work with thesis, there has been identified a number of subjects that would be interesting to conduct further work on. Some of would build on and some would add to the results of the thesis.

- More research and analysis with help of DIANA software is recommended to collect more data to be able to have an accurate and detailed results for the behavior of the box girder with failed tendons at the ultimate stage.
- Conducting the experiment on a much smaller element size mesh would significantly increase the accuracy of the results
- The obvious step would be to extend study using bond-slip reinforcement and then comparing the results with embedded reinforcement.
- It is recommended to have more research that would check and compare results from different finite analysis programs like DIANA, ANSYS or Abaqus

---

## Referanser

- [1] FEA DIANA and BV DIANA User's Manual Release. Diana10.3. *DIANA FEA: Delft, The Netherlands*, 2017.
- [2] Hikmet Süleymanoğlu, Almıla Uzel, and Güray Arslan. Use of post-tensioned concrete slabs for sustainable design of buildings. In *High Tech Concrete: Where Technology and Engineering Meet*, pages 2390–2395. Springer, 2018.
- [3] Jasmin Abdelhalim. Prestressed concrete slabs with bonded and unbonded tendons. 2021.
- [4] K Palacio. Practical recommendations for nonlinear structural analysis in diana. *TNO DIANA BV, Delft*, 2013.
- [5] TJ Van Dam, LL Sutter, KD Smith, MJ Wade, KR Peterson, et al. Guidelines for detection, analysis, and treatment of materials-related distress in concrete pavements. volume 2, guidelines description and use. Technical report, United States. Federal Highway Administration, 2002.
- [6] Max AN Hendriks, Ane de Boer, and Beatrice Belletti. Guidelines for nonlinear finite element analysis of concrete structures. *Rijkswaterstaat Centre for Infrastructure, Report RTD*, pages 1016–1, 2017.
- [7] Hedvig Vestad and Magnus Vestad. Non-linear behaviour of insufficiently grouted posttensioned concrete members. Master's thesis, NTNU, 2021.
- [8] Reinforced concrete beam: Simulation of an experimental test. page 57.
- [9] Ajinkya S Dixit and VG Khurd. Nonlinear flexural behavior of post tensioned beam. *International Journal for Research in Applied Science & Engineering Technology (IJRASET)*, ISSN, pages 2321–9653.
- [10] U Kim, PR Chakrabarti, and JH Choi. Nonlinear finite element analysis of unbonded post-tensioned concrete beams. In *Challenges, opportunities and solutions in structural engineering and construction*, pages 121–126. CRC Press, 2009.
- [11] A. de Boer M. Hendriks and B. Belletti. Guidelines for nonlinear finite element analysis of concrete structures. *Rijkswaterstaat Centre for Infrastructure, Report RTD:10161: 2017*, 2017.
- [12] Publikasjon nr.14 spennarmeringsarbeider. *Norsk betongforening*, 2016.
- [13] Møre og romsdal - vegliste spesialtransport - oktober 2021. *Statens vegvesen*, 2021.

- 
- [14] Statens vegvesen Vegdirektoratet. Bruklassifisering: lastforskrifter for klassifisering av bruer, 2014.
- [15] Naiwei Lu and Mohammad Noori. Reliability and serviceability of long span steel bridges under random traffic loads. 05 2017.

---

# Vedlegg

## A Appendix

### A Midspan deflection in three point bending test

The deflection  $\delta_F$  can be calculated using formula

$$f(x) = \frac{P(x)}{Q(x)}$$

$$\delta_F = \frac{1}{48} \frac{PL^3}{48EI}$$

### B Midspan deflection in four point bending test

The upward deflection  $\delta_P$  because of the prestressing moment MP , that is constant over the length of the beam, can be calculated using formula:

$$\delta_P = \frac{1}{EI} \int_L^0 M(x)M\bar{(x)} dx = \frac{1}{EI} \frac{1}{2} M\bar{M}L$$

$$\delta_P = \frac{1}{EI} \frac{1}{2} (Pe) \left(\frac{1}{4}L\right)L = \frac{1}{(8EI)} PeL^2$$

The self weight deflection  $\delta_g$  can be calculated using formula where  $g = A \cdot \gamma_c$ :

$$\delta_g = \frac{5}{384} \cdot \frac{gL^4}{EI}$$

The deflection  $\delta_F$  can be calculated using formula

$$\delta_c = \frac{Pa}{6EI} \cdot (3Lx - 3x^2 - a^2) \quad \text{where} \quad \delta_c = \delta\left(\frac{L}{2}\right)$$

$$\delta_c = \frac{Pa}{6EI} \cdot \left(\frac{3}{4}L^2 - a^2\right) = \frac{Pa}{24EI} \cdot (3L^2 - 4a^2)$$

---

## C Analytical calculations of the RC beam

As the RC beam is an ordinary concrete beam without posttensioning, it is subjected to pure bending. The point loads  $F$  and the self weight  $g$  are considered in the following calculations

### C.1 Deformations and cracking load of Stage I of the RC Beam

$$A_t = A_c + \eta(A_s + A'_s)$$
$$\eta = \frac{E_s}{E_c} = \frac{210000}{24800} = 8,47$$

The moment of the areas about the upper edge of the cross section gives the position of the neutral axis N.A. at the position  $\alpha d$ :

$$\alpha d = \frac{A_c \frac{h}{2} + \eta(A_s d + A'_s d')}{A_t}$$

$$\alpha d = mm$$

The bending stiffness  $EI_I$  for Stage I is:

$$EI_I = E_c I_c + E_s I_s + E_s I'_s$$
$$EI_I = N/mm^2$$

The cracking moment,  $M_{cr}$  and the corresponding cracking load  $F_{cr}$  can be found by the curvature relation:

$$\frac{1}{r} = \frac{M}{EI_I} = \frac{\epsilon_c^u}{(h - \alpha d)}$$

$$M_{cr} = \frac{\epsilon_c^u \cdot EI_I}{(h - \alpha d)}$$

$$M_{cr} = \frac{f_{ct} \cdot EI_I}{(h - \alpha d)}$$

---

## D Reinforcement

The bridge has 8 high-strength steel tendons, The coordinates of the polygon lines for the right part (north side) for box girder are listed below. The coordinates of the polygon lines for the left part (south side) are exactly the same except that the y axis values are negative. This is explained by the fact that the bridges is symmetrical. Function "mirror" was use to obtain the exact position of tendons for the south side of the bridge

---

Length(x)[mm]	Height(y)[mm]	Depth (z)[mm]
0	1909	150
2000	1910	153
4000	1915	178
6000	1926	228
8000	1943	303
10000	1964	402
12000	1992	527
14000	2025	677
16000	2063	851
18000	2107	1051
20000	2157	1275
22000	2211	1524
24000	2262	1753
26000	2298	1917
28000	2319	2015
30000	2327	2048

Tabell 14: Coordinates for defining the polyline for prestress tendon N1

Length(x)[mm]	Height(y)[mm]	Depth (z)[mm]
0	2116	220
2000	2217	223
4000	2122	247
6000	2133	295
8000	2148	367
10000	2169	463
12000	2196	583
14000	2228	727
16000	2265	895
18000	2307	1087
20000	2354	1304
22000	2407	1544
24000	2456	1764
26000	2490	1922
28000	2511	2016
30000	2518	2048

Tabell 15: Coordinates for defining the polyline for prestress tendon N2

---

Length(x)[mm]	Height(y)[mm]	Depth (z)[mm]
0	1953	350
2000	1954	354
4000	1961	387
6000	1975	452
8000	1997	551
10000	2026	682
12000	2062	846
14000	2105	1042
16000	2156	1272
18000	2213	1534
20000	2276	1818
22000	2329	2059
24000	2370	2247
26000	2400	2381
28000	2417	2461
30000	2423	2488

Tabell 16: Coordinates for defining the polyline for prestress tendon N3

Length(x)[mm]	Height(y)[mm]	Depth (z)[mm]
0	2160	350
2000	2161	354
4000	2168	387
6000	2181	452
8000	2202	551
10000	2230	682
12000	2264	846
14000	2305	1042
16000	2354	1272
18000	2409	1534
20000	2468	1818
22000	2519	2059
24000	2558	2247
26000	2587	2381
28000	2603	2461
30000	2609	2488

Tabell 17: Coordinates for defining the polyline for prestress tendon N4



---

## E Numerical studies of Sykkylsbrua

### E.1 Cross-Sectional Area

The area of the cross-section equal:

$$\Sigma A_{tot} = A_1 + A_2 + \dots + A_n$$

$$A_1 = 1750 \cdot 280 = 4,90 \cdot 10^5 mm^2$$

$$A_2 = \frac{1}{2} \cdot 468 \cdot 151 = 3,53 \cdot 10^4 mm^2$$

$$A_3 = \frac{1}{2} \cdot 2090 \cdot 450 = 4,70 \cdot 10^5 mm^2$$

$$A_4 = \frac{1}{2} \cdot 2420 \cdot 540 = 6,53 \cdot 10^5 mm^2$$

$$A_5 = \frac{1}{2} \cdot 330 \cdot 510 = 8,42 \cdot 10^4 mm^2$$

$$A_6 = 5000 \cdot 250 = 1,25 \cdot 10^6 mm^2$$

$$A_7 = 460 \cdot 275 = 1,27 \cdot 10^5 mm^2$$

$$A_{tot} = 2 \cdot 3,11 mm^2 = 6,22 \cdot 10^6 mm^2$$

### E.2 1. Areal of moment

The first moment of area is based on the mathematical construct moments in metric spaces. It is a measure of the spatial distribution of a shape in relation to an axis.

$$S_y = A\bar{x} = \Sigma_{i=1}^n x_i dA_i = \int_A x dA$$

$$S_{y1} = \left(\frac{1}{2} \cdot 280\right) \cdot 4,90 \cdot 10^5 = 6,86 \cdot 10^7 mm^3$$

$$S_{y2} = \left(\frac{1}{3} \cdot 151 + 280\right) \cdot 3,53 \cdot 10^4 = 1,17 \cdot 10^7 mm^3$$

$$S_{y3} = \left(\frac{1}{3} \cdot 2090\right) \cdot 4,70 \cdot 10^5 = 3,28 \cdot 10^8 mm^3$$

$$S_{y4} = \left(\frac{2}{3} \cdot 2420\right) \cdot 6,53 \cdot 10^5 = 1,05 \cdot 10^9 mm^3$$

$$S_{y5} = \left(\frac{2}{3} \cdot 300 + 2090\right) \cdot 8,42 \cdot 10^4 = 1,94 \cdot 10^8 mm^3$$

$$S_{y6} = \left(2450 + \frac{250}{2}\right) \cdot 1,25 \cdot 10^6 = 3,18 \cdot 10^9 mm^3$$

$$S_{y7} = 2808 \cdot 1,27 \cdot 10^5 = 3,55 \cdot 10^8 mm^3$$

$$S_y = \Sigma y_i = S_{y1} + S_{y7} + 2 \cdot (S_{y2} + S_{y3} + S_{y4} + S_{y5} + S_{y6} + S_{y8})$$

$$S_y = 2 \cdot (0,686 + 0,117 + 3,28 + 10,5 + 1,94 + 31,8 + 3,55) \cdot 10^8$$

$$S_y = 1,038 \cdot 10^{10} mm^3$$

### E.3 Area center

Geometric center of a plane figure is the arithmetic mean position of all the points in the figure.

$$z_c = \frac{S_y}{A} = \frac{1,038 \cdot 10^{10}}{6,22 \cdot 10^6} = 1669 mm$$

### E.4 Second moment of area

The second moment of area is needed if to relate the stress produced in a beam to the applied bending moment.

$$\text{Second moment of area} = \int_{-\frac{d}{2}}^{\frac{d}{2}} y^2 b dy = \frac{bd^3}{12}$$

$$I_{y1} = \frac{1750 \cdot 280^3}{12} = 3,20 \cdot 10^9 mm^4, \quad z_{c1} = \frac{280}{2} = 140 mm$$

$$I_{y2} = \frac{1}{3} \cdot \frac{468 \cdot 151^3}{12} = 4,47 \cdot 10^7 mm^4, \quad z_{c2} = 300 \frac{151}{3} = 330 mm$$

$$I_{y3} = \frac{1}{3} \cdot \frac{450 \cdot 2090^3}{12} = 1,14 \cdot 10^{11} mm^4, \quad z_{c3} = \frac{1 \cdot 2090}{3} = 697 mm$$

$$I_{y4} = \frac{1}{3} \cdot \frac{540 \cdot 2420^3}{12} = 2,13 \cdot 10^{11} mm^4, \quad z_{c4} = \frac{2 \cdot 2420}{3} = 1613 mm$$

$$I_{y5} = \frac{1}{3} \cdot \frac{510 \cdot 300^3}{12} = 5,09 \cdot 10^8 mm^4, \quad z_{c5} = 330 + \frac{2 \cdot 2090}{3} = 2310 mm$$

$$I_{y6} = \frac{5000 \cdot 250^3}{12} = 6,51 \cdot 10^9 mm^4, \quad z_{c6} = 2420 + \frac{250}{2} = 2545 mm$$

$$I_{y7} = \frac{10000 \cdot 280^3}{12} = 1,829 \cdot 10^{10} mm^4, \quad z_{c7} = 2808 mm$$

$$\begin{aligned}
I_y &= \Sigma(I_{yn} + (z_c - z_n)^2 \cdot bd) \\
I_y &= 2 \cdot ((3,2 \cdot 10^9 + (1669 - 140)^2 \cdot 1750 \cdot 280) \\
&\quad + (4,47 \cdot 10^7 + (1669 - 330)^2 \cdot 468 \cdot 151 \cdot \frac{1}{2}) \\
&\quad + (1,14 \cdot 10^{11} + (1669 - 697)^2 \cdot 450 \cdot 2090 \cdot \frac{1}{2}) \\
&\quad + (2,13 \cdot 10^{11} + (1669 - 1613)^2 \cdot 540 \cdot 2420 \cdot \frac{1}{2}) \\
&\quad + (5,09 \cdot 10^8 + (1669 - 2310)^2 \cdot 300 \cdot 510 \cdot \frac{1}{2}) \\
&\quad + (6,51 \cdot 10^9 + (1669 - 2545)^2 \cdot 5000 \cdot 250) \\
&\quad + (7,79 \cdot 10^8 + (1669 - 2808)^2 \cdot 460 \cdot 275) \\
I_y &= 2 \cdot (11,50 + 0,64 + 5,89 + 2,15 + 0,32 + 9,64 + 1,65) \cdot 10^{11} \\
I_y &= 6,36 \cdot 10^{12} mm^4
\end{aligned}$$

## E.5 Loads

The self-weight of the bridge is calculated from the average cross-section multiply by average density of concrete. The self-weight can be considered as a line load  $g$  along the span of the bridge. Calculations are shown below.

$$g = \gamma_c \cdot A = 24kN/m \cdot 6.21 \cdot 10^6 = 149kN/m$$

$$P = 149kN/m \cdot 30m = 4470kN$$

The following values have been selected for traffic load acting on the bridge

- **Heavy load:**  $10.4kN/m^2$
- **Light load:**  $6kN/m^2$
- **Pedestrian load:**  $2/m^2$

The traffic load can be considered as a line load  $g$  along the span of the bridge. Calculations are shown below.

$$Q = 10,4kN/m^2 \cdot 3 \cdot 30 + 6kN/m^2 \cdot 2 \cdot 30 + 2kN/m^2 \cdot 30 \cdot 2 = 1416kN$$

$$q = \frac{Q}{30m} = 47,2kN/m$$

---

## E.6 Statically Indeterminate Beam

The sections of the bridge that have been analyzed can be treated as statically indeterminate beam.

Static model of the span can be may be presented as a fixed-end beam ABC supports a concentrated load P at the midpoint

$$\begin{aligned}H_A = H_B = 0 \quad R_A = R_B = \frac{P}{2} \\M_A = M_B \quad (1 \text{ degree of indeterminacy}) \\M = \frac{Px}{2} - M_A \quad (0 \leq x \leq \frac{L}{2}) \\EI\nu'' = M = \frac{Px}{2} - M_A \quad (0 \leq x \leq \frac{L}{2})\end{aligned}$$

after integration, it is obtained

$$\begin{aligned}EI\nu' = \frac{Px^2}{4} - M_Ax + C_1 \quad (0 \leq x \leq \frac{L}{2}) \\EI\nu = \frac{Px^3}{12} - \frac{M_Ax^2}{2} + C_1x + C_2 \quad (0 \leq x \leq \frac{L}{2})\end{aligned}$$

boundary conditions

$$\nu(0) = 0 \quad \nu'(0) = 0$$

symmetric condition

$$\nu'(0) = 0$$

the constants  $C_1, C_2$  and the moment  $M_A$  are obtained

$$\begin{aligned}C_1 = C_2 = 0 \\M_A = \frac{PL}{8} = M_B\end{aligned}$$

the shear force and bending moment diagrams can be plotted thus the slope and deflection equations are

$$\begin{aligned}\nu' = -\frac{Px}{8EI}(L - 2x) \quad (0 \leq x \leq \frac{L}{2}) \\\nu = -\frac{Px^2}{48EI}(3L - 4x) \quad (0 \leq x \leq \frac{L}{2})\end{aligned}$$

the maximum deflection occurs at the center

$$\delta_{max} = -\nu(L/2) = \frac{PL^3}{192EI}$$

---

the point of inflection occurs at the point where  $M = 0$ , *i.e.*  $x = \frac{L}{4}$ , the deflection at this point is

$$\delta = -\nu(L/4) = \frac{PL^3}{384EI} \quad \text{which is equal} \quad \frac{\delta_{max}}{2}$$

## E.7 Displacement

The downward deflection  $\delta_g$  because of the self weight  $g$ :

$$\delta_{max} = -\nu(L/2) = \frac{PL^3}{192EI} = \frac{8940N \cdot 10^3 \cdot (60000mm)^3}{192 \cdot 6.36 \cdot 10^{12}mm^2 \cdot 38000N/mm^2} = 41.7mm$$

The downward deflection  $\delta_q$  because of the traffic load  $q$ :

$$\delta_{max} = -\nu(L/2) = \frac{PL^3}{192EI} = \frac{2832N \cdot 10^3 \cdot (60000mm)^3}{192 \cdot 6.36 \cdot 10^{12}mm^2 \cdot 38000N/mm^2} = 13.2mm$$

## E.8 Moment

## E.9 Prestressing force

$$P_{total} = 8 \cdot 0.8 \cdot S_{0.2} = 8 \cdot 0.8 \cdot 3170kN = 2536kN$$

$$F = S = 0.8 \cdot 25.36kN = 20.3MN$$

The parabolic shape over the midspan acts over a length of  $L_1 = L - 2x$  where  $x = 7250mm$ . The inflection point between parabolas are located at the neutral axis, at  $z_c = 1460mm$  above the lower part of the box girder.  $x$  is the deflection point from the supported edge of the bridge

$$q_1 = \frac{8P_{e1}}{L_1^2} = \frac{8 \cdot 20288kN \cdot 1420mm}{(45500mm)^2} = 111.3kN/m$$

$$q_2 = \frac{8P_{e2}}{2x^2} = \frac{8 \cdot 20288kN \cdot 598mm}{(2 \cdot 7250mm)^2} = 461.6kN/m$$

Both load are considered as a force  $P_{q1+q2}$  action at a midspan of the bridge

$$P_{q1+q2} \cdot x = (111.3kN/m \cdot 461.6kN/m) \cdot 7250mm = 4153.5kN$$

---

The momen because of  $q_1$  are:

$$M_{q_1.midspan} = -\frac{qL^2}{24} = \frac{111.3N/mm \cdot (60000mm)^2}{24} = -16695kNm$$

$$M_{q_1.support} = \frac{qL^2}{12} = \frac{111.3N/mm \cdot (60000mm)^2}{12} = 33390kNm$$

The momen because of  $q_2$  are:

$$M_{q_2.support} = R \cdot \frac{\frac{x}{2} \cdot (L - \frac{x}{2})^2}{L^2} = 4153.5 \cdot \frac{\frac{7250mm}{2} \cdot (60000mm - \frac{7250mm}{2})^2}{(60000mm)^2} = -13292kNm$$

$$M_{q_2.midspan} = 0$$

---

## F Drawings

These drawings have been taken from Statens Vegvesen's database BRUTUS.

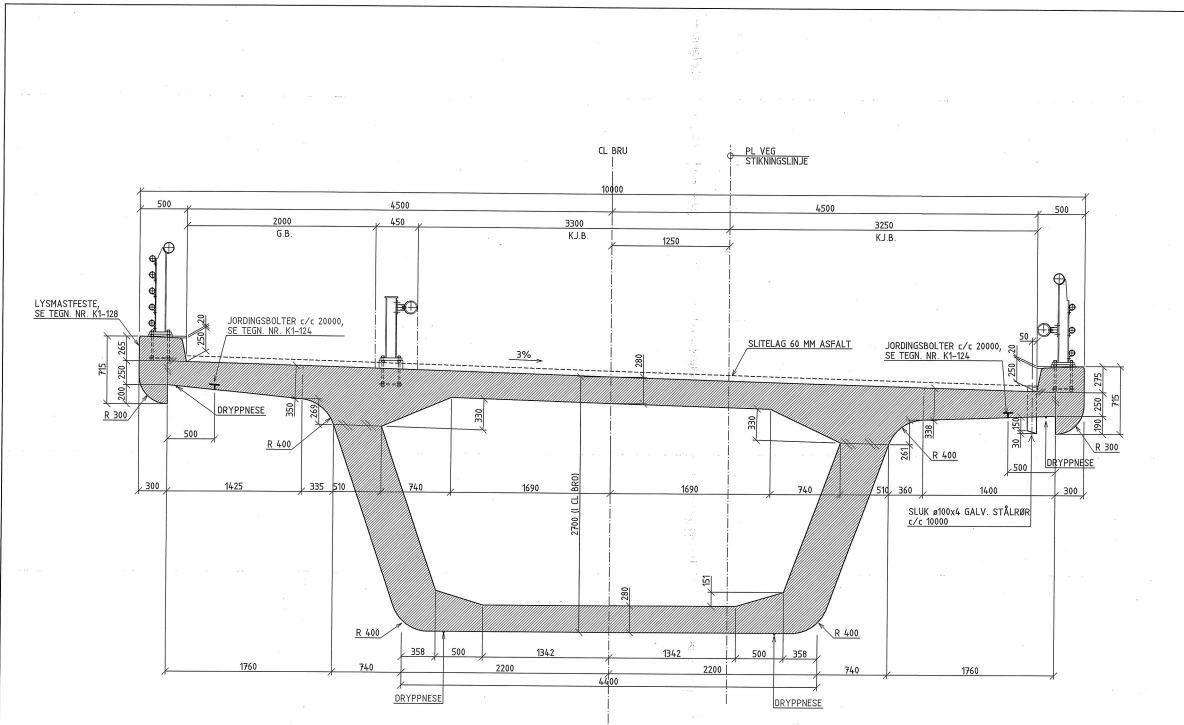
**Drawing 1:** Cross section of Sykkylvsbrua with notional lanes for carriageways

**Drawing 2:** Overview of Sykkylvsbrua, topology

**Drawing 3:** Passive reinforcement at the bottom of the bridge

**Drawing 4:** Passive reinforcement at the top of the bridge

**Drawing 5:** Shape of tendons between supports



TYPISK TVERRSNITT  
1:20

FORKLARINGER

BESTEMMELSER

1. LASTFORSKRIFTER FOR BRUER OG FERJEKAIER I DET OFFENTLIGE VEGNETT, DATERT 1995.
2. BETONG: FASTHETSKLASSE C35 SV-44/355 SV-30 MILJØKLASSE, NEGET AGGRESSIVT (M1) POREVOLUM:  $\leq 15\%$ .
3. KONTROLLKLASSE: UTVIDET KONTROLL IFØLGE NS 3420.
4. ARMERING: B500C, NS 3576.
5. SLITELAG: 60 mm ASFALT.

K1-115 D

HENVISNINGER

- |                          |                        |
|--------------------------|------------------------|
| 1. OVERSIKT              | SE TEGN NR. K1-100     |
| 2. OVERBYGNING           | SE TEGN NR. K1-116-122 |
| 3. JORDINGSBOLTER        | SE TEGN NR. K1-124     |
| 4. LYSMÅSTER             | SE TEGN NR. K1-128     |
| 5. REKKVERK G/S-VÆG      | SE TEGN NR. K1-129     |
| 6. REKKVERK IK KJØREBANE | SE TEGN NR. K1-130     |
| 7. REKKVERK IK KJØREBANE | SE TEGN NR. K1-131     |

SOM BYGGET 30.03.01

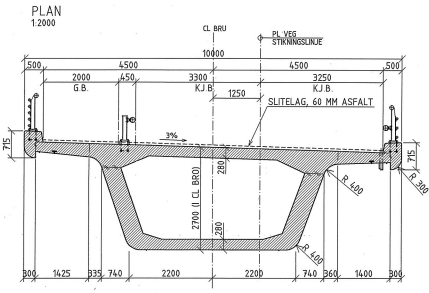
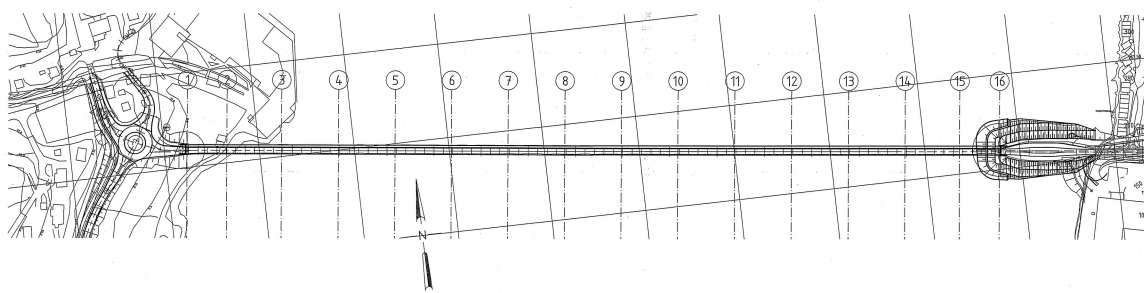
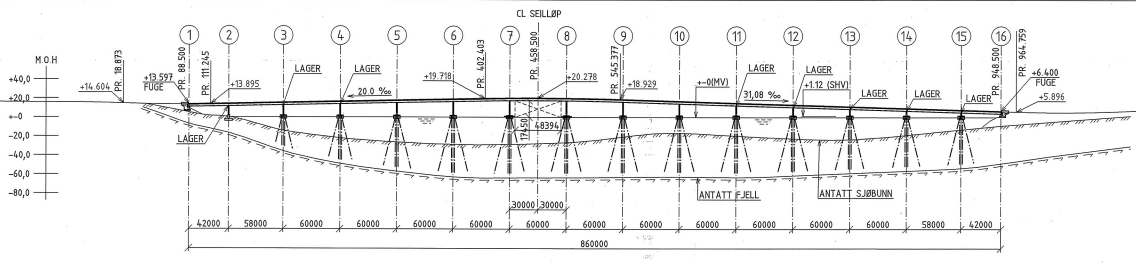
Godkjent som arbeidsføring følge brev fra Vegkontoret, datert 18.12.99  
Lars Tjørndal 22.10.99

D	ANLEGGSTEKNING	22.10.99	A/P
C	MÅL KOPPIERT	21.04.99	A/P
B	REVIDERT ANLEGGSTEKNING	15.02.99	A/P
A	ANLEGGSTEKNING	28.09.99	A/P
T	REKVVÆRK EBNET	22.10.99	A/P
Rev.	Rev.	Rev.	Rev.
Originaltekst	konstruert i	Rev.	Rev.
Sistene tegnet av Mera og Rønneid		Rev.	Rev.
		Proj. nr.	Rev.
ANLEGG: Fv. 71 SYKKYLVSBRIUA		3126300	02.10.98
PARSELL: BRUBANE TVERRSNITT		Rev.	SOM VIST
BYGGEPLAN: BRUBANE TVERRSNITT		Rev.	K1-115 D
FORN		Rev.	

0. VIKTIGHETSOMRÅDE: BRUBANE TVERRSNITT



PROFIL NR	0	100	200	300	400	500	600	700	800	900	1000	1100
PROFIL HØYDE	15.15	13.91	15.67	17.67	19.67	19.97	17.23	14.12	11.02	7.91	5.21	7.65
VERTIKALKURVE		R=1850	20.00%		R=2800			-31.08%			R=1500	
HORISONTALKURVE												



**FORKLARINGER**

**BESTEMMELSER**

1. LASTFORSKRIFTER FOR BRUER OG FERJEKAIER (DET OFFENTLIGE VEGNETT, DATERT 1995)
2. BETONG: FASTHETSKLASSE C35 SIV-40/C35 SIV-30. UNDER VANN: C35 (AUV) MILJØKLASSE: MEGET AGRESSIVT (MA). POREVOLUM: 5-12.5%
3. KONTROLLKLASSE: UTVIDET KONTROLL IFØLGE NS 3420.
4. ARMERING: B500C, NS 3576.
5. STÅL I PELER: S355J2G3
6. STÅL I LEEVEVERK: S355J2G3
7. SLITELAG: 60 mm ASFALT

**HENVISNINGER**

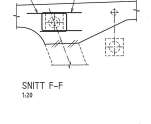
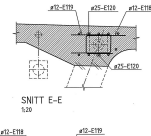
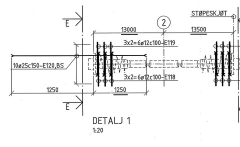
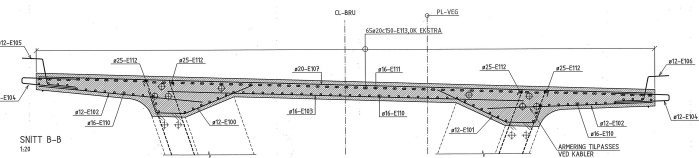
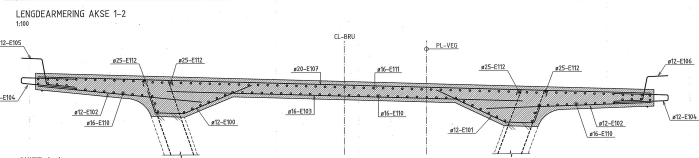
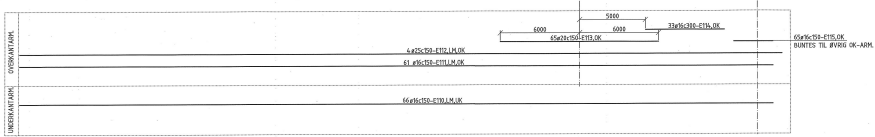
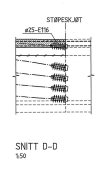
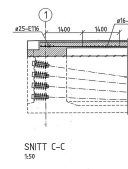
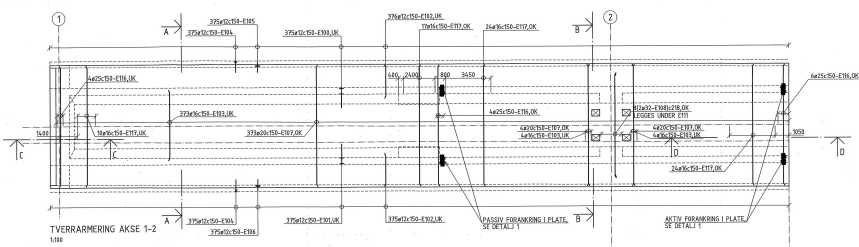
1. FUNDAMENT AKSE 2 SE TEGN. NR. K1-107
2. FUNDAMENT AKSE 3-15 SE TEGN. NR. K1-109
3. LEEVEVERK AKSE 7 OG 8 SE TEGN. NR. K1-112
4. SØTLER SE TEGN. NR. K1-113
5. TYPISK TVERRSNITT SE TEGN. NR. K1-115

SOM BYGGET 30.03.01

Godkjent som arbeidstegning ifølge brev fra Vegvesen, datert 18.10.99

C	ANBEIREDNING	12.10.95	AP	JGS
B	REVIDERT ANBEIREDNING	01.02.99	AP	JGS
A	ANBEIREDNING	28.10.98	AP	JGS
DR	DRIFTSKARTER (SISTEM) /			
DR	Støtting, vegvesen			
DR	Mere og Romsdøl			
DR				
Norconsult		3126300		
ANLEGG: Fv. 71 SYKKYLVESBRUA				
BYGGEPLAN: BETONGALTERNATIV OVERSKILT				
Tegn. nr.			SOM VIST	
Tegn. nr.			K1-100	D





**FORKLARINGER**

- BESTEMMELSER**
- ADNING: B500C
  - UTVEKSLING: ØA = 10K PELLUM STEG 55x55 mm TL KONSTRUKTIV ADNING 4x45 mm TL ROSTERINGSLEGN
  - UTVEKSLING: ØA = 10K PELLUM STEG 55x55 mm TL KONSTRUKTIV ADNING 4x45 mm TL ROSTERINGSLEGN
  - MONTERINGSJERN: MÅKS #10
  - OPPRING: 100x
  - LENGDEADNINGEN ER LISTET UT I LØPETER OG I. FOR ALL ØPENSADNINGER SKAL SKURTENE FORSTYKES IKT. 100/100.

K1-142 C

- HENVISNINGER**
- OVERSIKT SE TEKN NR. K1-100
  - SE OG STEG AKSE 1-2, ADNING SE TEKN NR. K1-101
  - BEVILJESTE DRG: E10-E12

SOM BYGGET 30.03.01

1	FAKTORETTING	SE TEKN F. 10.1
2	REVISJONER	SE TEKN F. 10.1
3	UTVEKSLING AV ADNING	SE TEKN F. 10.1
4	UTVEKSLING AV ADNING	SE TEKN F. 10.1
5	UTVEKSLING AV ADNING	SE TEKN F. 10.1
6	UTVEKSLING AV ADNING	SE TEKN F. 10.1
7	UTVEKSLING AV ADNING	SE TEKN F. 10.1
8	UTVEKSLING AV ADNING	SE TEKN F. 10.1
9	UTVEKSLING AV ADNING	SE TEKN F. 10.1
10	UTVEKSLING AV ADNING	SE TEKN F. 10.1
11	UTVEKSLING AV ADNING	SE TEKN F. 10.1
12	UTVEKSLING AV ADNING	SE TEKN F. 10.1
13	UTVEKSLING AV ADNING	SE TEKN F. 10.1
14	UTVEKSLING AV ADNING	SE TEKN F. 10.1
15	UTVEKSLING AV ADNING	SE TEKN F. 10.1
16	UTVEKSLING AV ADNING	SE TEKN F. 10.1
17	UTVEKSLING AV ADNING	SE TEKN F. 10.1
18	UTVEKSLING AV ADNING	SE TEKN F. 10.1
19	UTVEKSLING AV ADNING	SE TEKN F. 10.1
20	UTVEKSLING AV ADNING	SE TEKN F. 10.1
21	UTVEKSLING AV ADNING	SE TEKN F. 10.1
22	UTVEKSLING AV ADNING	SE TEKN F. 10.1
23	UTVEKSLING AV ADNING	SE TEKN F. 10.1
24	UTVEKSLING AV ADNING	SE TEKN F. 10.1
25	UTVEKSLING AV ADNING	SE TEKN F. 10.1
26	UTVEKSLING AV ADNING	SE TEKN F. 10.1
27	UTVEKSLING AV ADNING	SE TEKN F. 10.1
28	UTVEKSLING AV ADNING	SE TEKN F. 10.1
29	UTVEKSLING AV ADNING	SE TEKN F. 10.1
30	UTVEKSLING AV ADNING	SE TEKN F. 10.1
31	UTVEKSLING AV ADNING	SE TEKN F. 10.1
32	UTVEKSLING AV ADNING	SE TEKN F. 10.1
33	UTVEKSLING AV ADNING	SE TEKN F. 10.1
34	UTVEKSLING AV ADNING	SE TEKN F. 10.1
35	UTVEKSLING AV ADNING	SE TEKN F. 10.1
36	UTVEKSLING AV ADNING	SE TEKN F. 10.1
37	UTVEKSLING AV ADNING	SE TEKN F. 10.1
38	UTVEKSLING AV ADNING	SE TEKN F. 10.1
39	UTVEKSLING AV ADNING	SE TEKN F. 10.1
40	UTVEKSLING AV ADNING	SE TEKN F. 10.1
41	UTVEKSLING AV ADNING	SE TEKN F. 10.1
42	UTVEKSLING AV ADNING	SE TEKN F. 10.1
43	UTVEKSLING AV ADNING	SE TEKN F. 10.1
44	UTVEKSLING AV ADNING	SE TEKN F. 10.1
45	UTVEKSLING AV ADNING	SE TEKN F. 10.1
46	UTVEKSLING AV ADNING	SE TEKN F. 10.1
47	UTVEKSLING AV ADNING	SE TEKN F. 10.1
48	UTVEKSLING AV ADNING	SE TEKN F. 10.1
49	UTVEKSLING AV ADNING	SE TEKN F. 10.1
50	UTVEKSLING AV ADNING	SE TEKN F. 10.1
51	UTVEKSLING AV ADNING	SE TEKN F. 10.1
52	UTVEKSLING AV ADNING	SE TEKN F. 10.1
53	UTVEKSLING AV ADNING	SE TEKN F. 10.1
54	UTVEKSLING AV ADNING	SE TEKN F. 10.1
55	UTVEKSLING AV ADNING	SE TEKN F. 10.1
56	UTVEKSLING AV ADNING	SE TEKN F. 10.1
57	UTVEKSLING AV ADNING	SE TEKN F. 10.1
58	UTVEKSLING AV ADNING	SE TEKN F. 10.1
59	UTVEKSLING AV ADNING	SE TEKN F. 10.1
60	UTVEKSLING AV ADNING	SE TEKN F. 10.1
61	UTVEKSLING AV ADNING	SE TEKN F. 10.1
62	UTVEKSLING AV ADNING	SE TEKN F. 10.1
63	UTVEKSLING AV ADNING	SE TEKN F. 10.1
64	UTVEKSLING AV ADNING	SE TEKN F. 10.1
65	UTVEKSLING AV ADNING	SE TEKN F. 10.1
66	UTVEKSLING AV ADNING	SE TEKN F. 10.1
67	UTVEKSLING AV ADNING	SE TEKN F. 10.1
68	UTVEKSLING AV ADNING	SE TEKN F. 10.1
69	UTVEKSLING AV ADNING	SE TEKN F. 10.1
70	UTVEKSLING AV ADNING	SE TEKN F. 10.1
71	UTVEKSLING AV ADNING	SE TEKN F. 10.1
72	UTVEKSLING AV ADNING	SE TEKN F. 10.1
73	UTVEKSLING AV ADNING	SE TEKN F. 10.1
74	UTVEKSLING AV ADNING	SE TEKN F. 10.1
75	UTVEKSLING AV ADNING	SE TEKN F. 10.1
76	UTVEKSLING AV ADNING	SE TEKN F. 10.1
77	UTVEKSLING AV ADNING	SE TEKN F. 10.1
78	UTVEKSLING AV ADNING	SE TEKN F. 10.1
79	UTVEKSLING AV ADNING	SE TEKN F. 10.1
80	UTVEKSLING AV ADNING	SE TEKN F. 10.1
81	UTVEKSLING AV ADNING	SE TEKN F. 10.1
82	UTVEKSLING AV ADNING	SE TEKN F. 10.1
83	UTVEKSLING AV ADNING	SE TEKN F. 10.1
84	UTVEKSLING AV ADNING	SE TEKN F. 10.1
85	UTVEKSLING AV ADNING	SE TEKN F. 10.1
86	UTVEKSLING AV ADNING	SE TEKN F. 10.1
87	UTVEKSLING AV ADNING	SE TEKN F. 10.1
88	UTVEKSLING AV ADNING	SE TEKN F. 10.1
89	UTVEKSLING AV ADNING	SE TEKN F. 10.1
90	UTVEKSLING AV ADNING	SE TEKN F. 10.1
91	UTVEKSLING AV ADNING	SE TEKN F. 10.1
92	UTVEKSLING AV ADNING	SE TEKN F. 10.1
93	UTVEKSLING AV ADNING	SE TEKN F. 10.1
94	UTVEKSLING AV ADNING	SE TEKN F. 10.1
95	UTVEKSLING AV ADNING	SE TEKN F. 10.1
96	UTVEKSLING AV ADNING	SE TEKN F. 10.1
97	UTVEKSLING AV ADNING	SE TEKN F. 10.1
98	UTVEKSLING AV ADNING	SE TEKN F. 10.1
99	UTVEKSLING AV ADNING	SE TEKN F. 10.1
100	UTVEKSLING AV ADNING	SE TEKN F. 10.1

BYGGEPÅN BRUPLATE AKSE 1-2  
PLAN NR. SNITT  
ADNING

